2018

IMPROVING HELICAL ANCHOR EFFICIENCY: ANALYTICAL MODELING

Lars Hildebrandt
University of Rhode Island, lars-hildebrandt@gmx.de

IMPROVING HELICAL ANCHOR EFFICIENCY:

ANALYTICAL MODELING

BY

LARS HILDEBRANDT

A THESIS SUBMITTED IN PARTIAL FULFILLMENT OF THE

REQUIREMENTS FOR THE DEGREE OF

MASTER OF SCIENCE

IN

CIVIL AND ENVIRONMENTAL ENGINEERING

UNIVERSITY OF RHODE ISLAND

2018

MASTER OF SCIENCE

OF

LARS HILDEBRANDT

APPROVED:

Thesis Committee:

Major Professor Aaron S. Bradshaw

Christopher D. P. Baxter

David Taggart

Nasser H. Zawia
DEAN OF THE GRADUATE SCHOOL

UNIVERSITY OF RHODE ISLAND
2018

ABSTRACT

Helical anchors (or helical piles) are currently being considered for anchorage of floating offshore wind turbine platforms. Maximizing the geotechnical efficiency of these types of anchors will help to minimize the overall cost of the mooring system. One measure of efficiency of a helical anchor is the torque factor, defined as the ratio of the pullout capacity to the installation torque. The objective of this study is to evaluate available analytical models from the literature that may be used to predict the torque factor of a helical pile, consisting of a pipe pile with a single helix attached to the bottom. Three different analytical models were evaluated using data collected from small-scale load tests on helical piles in sand. The models included Ghaly & Hanna (1991), Perko (2001), and Tsuha & Aoki (2010). Interface shear tests were also performed to characterize the residual interface friction angle for the small-scale anchor tests. Both the Ghaly & Hanna (1991) and Perko (2001) models tended to overpredicted the measured torque factors in most cases with significant variability. The Tsuha & Aoki (2010) model yielded the best predictions, which only requires the dimensions of the helix and the residual interface friction angle of the foundation soil.

ACKNOWLEDGMENTS

The last year at URI in the United States has been an amazing experience for me. It was very interesting for me to be here, both, professionally and personally. I want to thank everyone who made this year so special for me.

This thesis would not have been possible for me without my Major Advisor, Aaron Bradshaw. I really want to thank you for putting so much effort in helping me to finish my thesis. Your enthusiasm always motivated me and made every topic we talked about always very interesting for me; even if it was about springs. I will never forget the first preparations and experiments we did together outside, which never felt like work, even if it was. Also, in the office part, I am very thankful for you being there, answering all questions I had, and giving me advises which lead me into the right direction. Last but not least, I would like to thank you for funding my education here at URI.

I also want to thank Christopher Baxter for his support in instructing and explaining all about Shear Tests, which have been a great part of my research. Thank you for all your patience, knowledge, explanations, and enthusiasm you provided to help me. Thanks to your good mood, the working atmosphere in your lab has always been great, and I really liked to come here to work on my thesis. Also, personally, I thank you for showing me American traditions by inviting me to your Thanksgiving dinner, which I really enjoyed.

Furthermore, I would like to thank my committee member David Taggart for the support he provided to help me with research related questions, as well as Reza Hashemi for acting as chairman in my defense.

Also, I thank Gail Paolino, Fred Pease, and Robin Freeland for their support in helping me with my research project, both, practical, and organizational. Especially, thank you Fred for providing your workshop skills. You supplied a great contribution to my shear tests, which would not have been possible, without you and the module you built for me.

Also, I am very thankful for my office mates Maeve Story, Paul Sauco, Robin Zuelke, Ryan Lozinski, and Sam Lindgren. Thank you for helping us with all our tests we had to conduct outside, without you it would not have been possible to work on our research project. Also, it was always fun to come into the office, we had a lot of fun. Especially, I want to thank you, Robin, for working with me on this project. The tests and the preparations we had to make were exhausting in parts, but together with you, we always found a way to make it as comfortable as possible.

Last but not least, I want to thank my whole family for all the support they gave me. Thank you, Mom and Dad, for always being there and supporting me in my professional as well as in my private path of life. I really appreciate all you have ever done for me. Also, thank you Jane, especially for, regarding the past year, being a great inspiration and example for me in taking the chance of studying abroad.

TABLE OF CONTENTS

LIST OF TABLES

LIST OF FIGURES

CHAPTER 1: INTRODUCTION

Helical anchors, also known as screw anchors or helical piles, are used in a variety of civil engineering applications and consist of one or more helical shaped circular plates affixed to a central hub as shown in Figure 1.

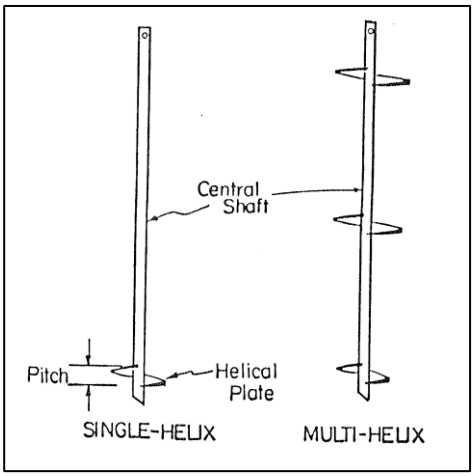

Figure 1: Single and multi-helical piles (Clemence et. al 1994)

As foundations they have been used, for example, for transmission towers, structural underpinning, and as boat anchors. There is current interest in the viability of using helical anchors to moor large floating offshore wind turbine platforms in deep water.

The installation process requires a torque and a downward 'crowd' force to screw the anchors into the ground. These forces are typically applied using a hydraulically powered driver. The required power of the driver depends on the torque required to screw the pile into the soil. The proportional installation costs of helical piles are significant, especially for offshore projects. Greater efficiencies of these anchors may be achieved by lowering the installation forces while maximizing their pullout capacity.

The proposed study is part of an overall research study aimed at finding ways to improve the efficiency of helical piles. This work complements the physical model testing of helical piles that is presented in a separate MS thesis written by Robin Zuelke. The physical modeling study was aimed at finding modifications that could be done to a helical pile to reduce installation torque while maximizing capacity. This thesis will focus on analytical modeling of the interaction between the helical anchor materials and foundation soil. Accurate analytical models will help in the design and optimization of helical anchors for offshore applications in the future.

Chapter 2 will provide background information about available models in the literature that correlate uplift capacity to installation torque. These models will be evaluated in a later chapter. Chapter 3 focuses on interface shear testing to obtain the interface friction angle between the test sand and different materials, namely steel, sandpaper, and Teflon. The resulting parameters will be used as input in the modeling efforts. In Chapter 4 the models are evaluated based on comparison to the physical model test data. Finally, Chapter 5 summarizes the results and gives recommendations for further studies.

CHAPTER 2: LITERATURE REVIEW

This chapter presents a review of the literature that is relevant to this thesis. It includes a review of analytical modeling of helical anchors/piles and the measurement of interface friction angle.

2.1 Analytical Modeling of Helical Piles

Models for Pullout Capacity

Clemence et. al (1994) explain two different approaches to predict the uplift capacity of multihelix anchors in sand. These two approaches are based on either the cylindrical shear or the individual plate bearing methods (Figure 2).

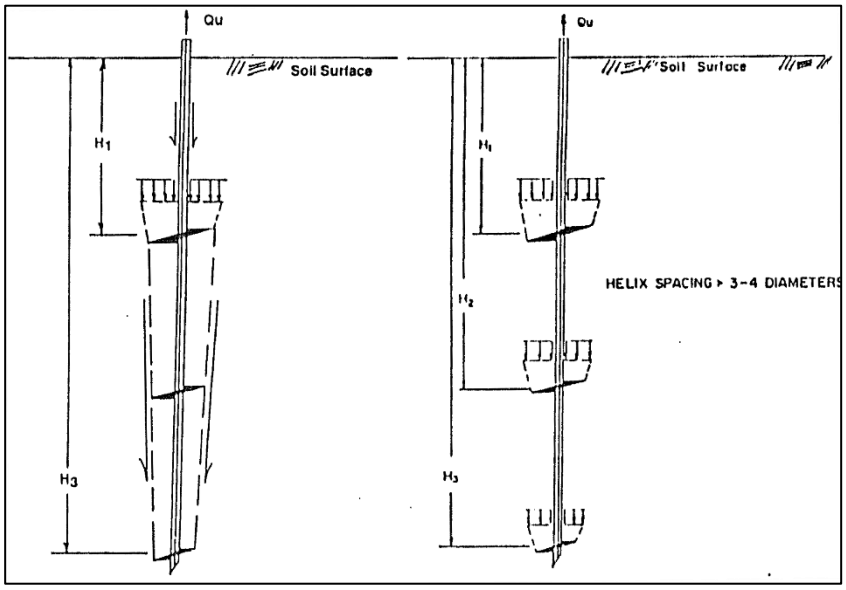

Figure 2: Failure surfaces for helical anchors Clemence et. al (1994)

The cylindrical shear method assumes that the helical plates form a cylindrical shear surface in the middle along the anchor. The capacity can be estimated by the shearing resistance of the soil along the cylinder and by the uplift resistance of the top helix. In contrast, the individual plate bearing method assumes that the resistance of the anchor is the sum of the bearing capacity provided by each plate where the failure occurs.

Clemence et. al use five analytical methods proposed by different authors to predict the uplift capacity and compare them to field measurements. The most accurate estimation is given by the A.B. Chance individual plate method using an uplift capacity factor for sands N_q. Other methods include the anchor shaft friction which may provide very little resistance at least for smaller shaft sizes. The A.B. Chance torque method uses a torque factor K_t, which correlates the uplift capacity (Q_u) to an average required installation torque value (T) for the final distance of penetration, which underpredicted the capacity in all cases. The torque factor relates the capacity and the installation torque as follows:

(1) $$Q_u = K_t * T$$

where Q_u=ultimate capacity, K_t=torque factor, and T=installation torque. However, using an empirical value of 20, a good match (within 5 %) between prediction and actual load resistance was obtained. The authors conclude that a relationship exists between installation torque and uplift capacity.

The findings by Clemence et al. (1994) are consistent with those by Hoyt and Clemence (1989) who analyzed numerous helical anchor tests from literature and determined the uplift capacity by applying the three different approaches. They found statistical

evidence that the torque correlation method is a little more consistent than either of the individual bearing and cylindrical shear methods. Table 1 summarizes the minimum, maximum, mean, and median values and standard deviations of the capacity ratios of the actual to the calculated uplift capacity (Q_{act}/Q_{calc}).

Table 1: Comparison of uplift capacity ratios (Q_{act}/Q_{calc}) of different approaches

Method	***Min.***	***Max.***	***Mean***	***Std. Dev***	***Median***
Cyl. Shear	0.07	7.29	1.50	1.18	1.15
Ind. Bearing	0.03	7.04	1.56	1.28	1.26
Inst. Torque	0.30	4.67	1.49	0.88	1.30

Models for Installation Forces

The Energy Method proposed by Perko (2001) predicts the installation torque of helical anchors based on energy exerted during installation, which is required to displace the helical anchor once in place. This method avoids the relation of torque measurement with angle of friction and cohesion of the soil due to the complex interaction. It relates bearing and pullout capacity directly to installation torque by the equivalence of energy and takes downward force during installation, helical blade geometry, multiple helices, blade pitch per revolution, and hub radius into account.

The derivation of the method is based on the following postulate: “For local shear, penetration energy is proportional to the volume of soil displaced times the distance

displaced". Perko derives the following equation 2, which relates installation torque to the pullout capacity (Q) of a helical anchor:

(2) $$Q = \frac{12d(2\pi T + Fp)[r^2 + \sum_m (R_m^2 - r^2)]}{3[2r^3 p + \sum_n (R_n^2 - r^2) t_n^2] + 16\pi\alpha[3r^3\lambda + \sum_m (R_m^3 - r^3) t_m]},$$

where d=displacement during loading, T=installation torque, F=downward force exerted during installation, p=pitch per revolution, R_m=radius of m^{th} helical blade, r=radius hub, R_n=radius of n^{th} cutting blade, t_n=thickness of n^{th} cutting blade, α=ratio of side shear stress to penetration resistance, λ=length of hub, and t_m=thickness of m^{th} helical blade.

Perko compared capacity-torque ratios predicted by the proposed model with values obtained empirically by Hoyt and Clemence (1989), which matched them fairly well. Both models predict that the capacity-torque ratio decreases for increasing blade radii and (or) increasing hub radii. Also, Perko compared predicted values with field and laboratory data published in the literature to further verify the model. The data have a wide variety of helix pier sizes and geometries, from small scale laboratory tests to full scale field tests. The comparison is shown in Figure 3 where the diagonal line represents a 1:1 correlation between predicted and measured values of K_t.

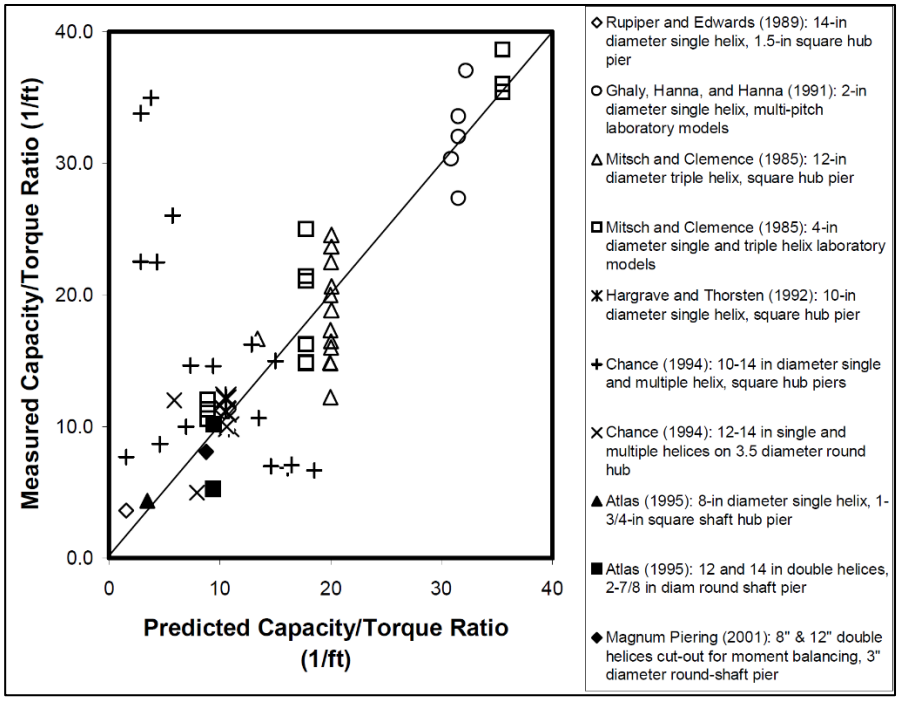

Figure 3: Comparison of the energy model with measured values from literature (Perko 2001).

The values predicted by the energy method match the general range and trend of field measurements quite well. Perko finds that K_t is relatively insensitive for changes in downward force during installation, final installation torque, number of independent cutting blades, total number of helical blades, and blade pitch. Furthermore, K_t is moderately affected by helical blade radius and strongly affected by hub diameter and blade thickness.

Ghaly and Hanna (1991) put a focus on the forces interacting between the soil and the anchor surface. They conducted experimental and theoretical studies on the torque required to install anchors. For their experiments, they used five different anchors varying in geometry and installed them into loose, medium, and dense sand in different

depths. The three single blade anchors just varied in the pitch height (10, 15, and 20 mm) by constant blade diameter, tie rod diameter, and blade thickness and the two multihelix anchors in the pitch height. After conducting the installation, they found that the required installation torque increased with the relative density of the sand and (or) the installation depth. Furthermore, an increase of the pitch to diameter ratio (p/B) of the anchor (i.e. the helix angle) increased the required installation torque to install an anchor to a given depth into sands with similar characteristics.

After conducting the pullout test they found that higher values of required installation torque (i.e. higher p/B ratios) lead to higher pullout capacities (Q_u). Hence, for the development of a theoretical model which predicts the required installation torque (T) and the crowd force (V) to install anchors, Ghaly and Hanna concentrated on the effect of the p/B ratio, helix angle, and general screw configuration which eliminate other factors that influence the anchors during installation. Figure 4 shows the acting forces on a single pitch screw anchor which are considered for the model, with: $T = \sum_{i=1}^{n} T_i$ and $V = \sum_{i=1}^{n} V_i$

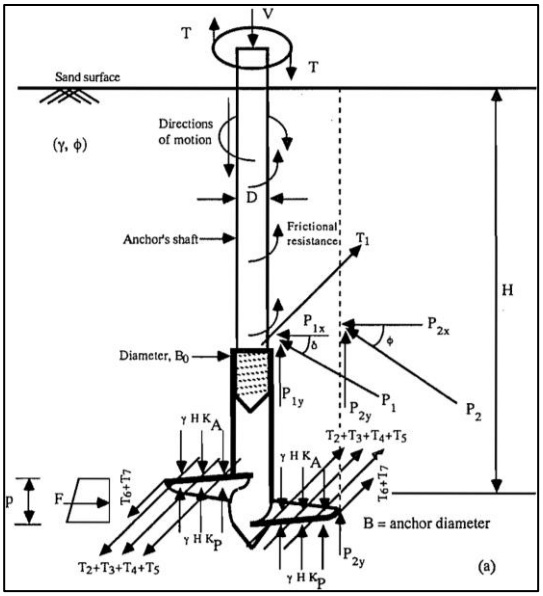

Figure 4: Forces acting on single pitch screw anchors during installation (Ghaly and Hanna 1991)

The comparison of the experimental and the theoretical values predicted by the proposed model for single pitch screw anchors are very consistent (Figure 5: exemplary for p=15mm). No data were presented for the crowd force.

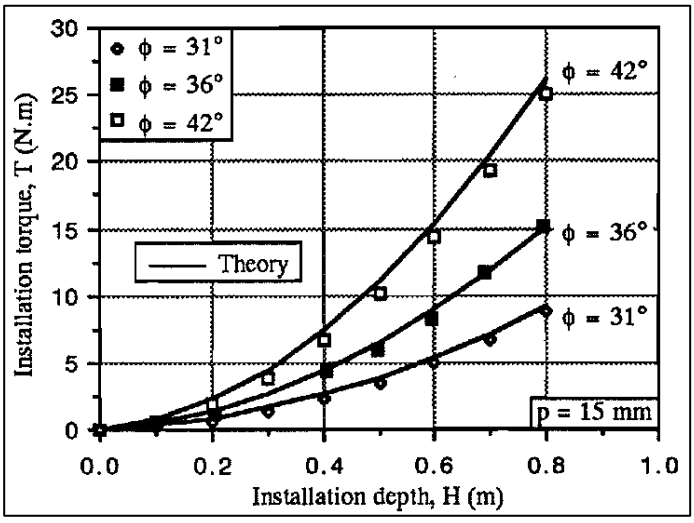

Figure 5 Comparison of theoretical and experimental torque results (Ghaly and Hanna 1991)

Furthermore, a relationship between the installation torque and the uplift capacity is found by plotting an established torque factor $F_t = \left[\frac{T}{\gamma AHp}\right]$ (similar to the uplift capacity factor Nq_u) against the corresponding Nq_u ($= \frac{Q_u}{\gamma AH}$) values. The plot for the single screw anchors is shown in Figure 6.

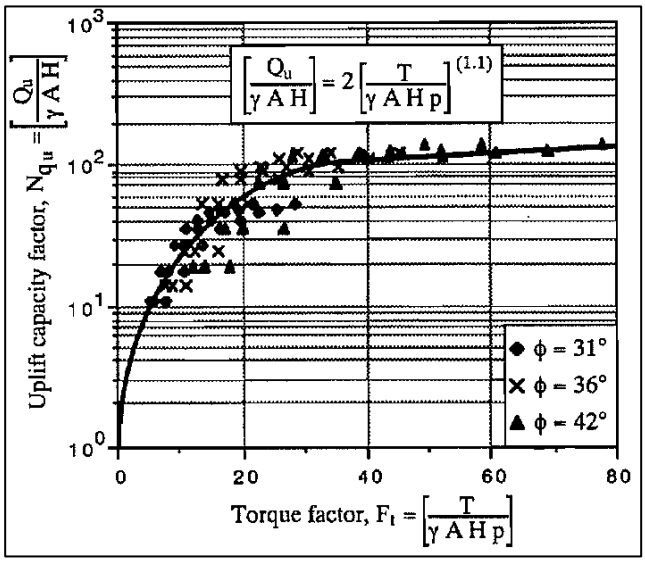

Figure 6: Relationship between uplift capacity and torque factor (Ghaly and Hanna 1991)

The equation of the curve is $\left[\frac{Q_u}{\gamma AH}\right] = \left[\frac{T}{\gamma AHp}\right]^{(1.1)}$ for single pitch screw anchors. The results of the theoretical model are very consistent with those of the experiments and somewhat consistent with those of the literature.

Tsuha and Aoki (2010) developed a theoretical model to relate the uplift capacity of an anchor to the required installation torque to install it. Compared to Ghaly and Hanna (1991), they take a closer look at the direct interaction between the soil in its properties

and the anchor surface. They used the model proposed by Tsuha (2007) based on the following scheme for three-helix piles (Figure 7).

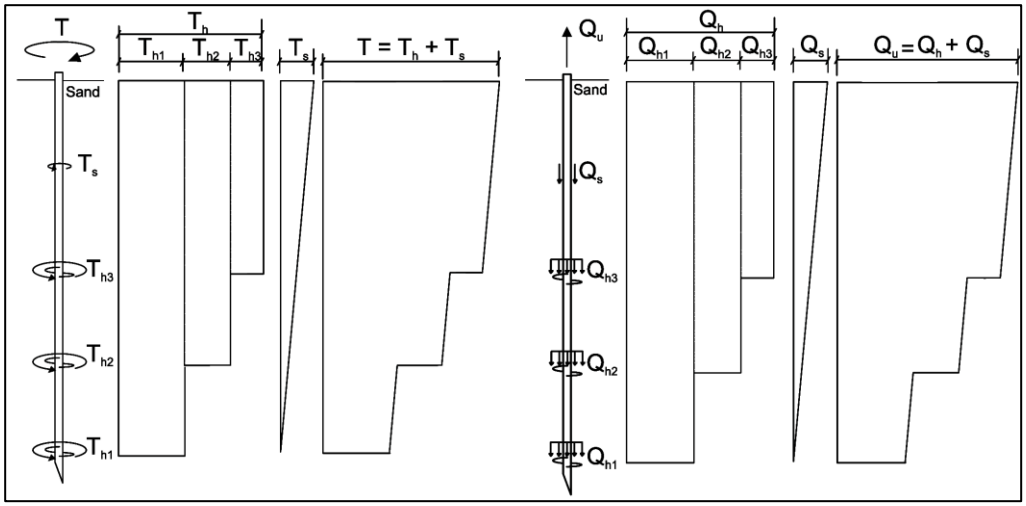

Figure 7: Driving and resisting moments acting during pile installation (left), forces resisting to the upward movement (right) (Tsuha and Aoki 2010)

Tsuha assumed that the required installation torque (T) is the sum of the resisting moments of the shaft (T_S) and the helices (T_h). The uplift capacity (Q_U) can be calculated in a similar way by addition of the shaft resistance (Q_S) and the uplift helix bearing capacity (Q_h) which is based on the A.B. Chance Co. method where failure occurs above each individual helix. A theoretical relationship between Q_u and T was found in the form of:

$$(3) \qquad Q_u = [Q_s] + [Q_h] = \left[\frac{2T_s}{d}\right] + \left[\frac{2T_h}{d_c \tan(\theta+\delta_r)}\right]$$

where Q_u=ultimate uplift capacity, Q_s=shaft reistance, Q_h=uplift helix bearing reistance, T_s=resisting moment of the shaft, T_h= resisting moment of the helices, d= shaft external

diameter, d_c=helix surface area, θ= helix angle, and δ_r=residual interface friction angle. For estimating Q_h, Tsuha uses the theoretical model by Ghaly and Hanna (1991), which assumes that the applied torque is resisted by a system of forces acting on the surfaces of the helices, which are directly in contact with the sand. To estimate T_h, a relationship to Q_h is derived by applying a mechanism of power screws, adapted for helical piles. The derived equation for Q_h depends on the helix angle (θ), the helix surface area (d_c), and the residual interface friction angle (δ_r) between the helix material and sand and can be used for anchors with one or more helical plates. Tsuha and Aoki validate the proposed model with help of centrifuge and direct shear interface tests.

The centrifuge tests were conducted to obtain values for Q_h and T_h by installing twelve different piles into two different sands just varying in density. The values for Q_S were not measured because of the risk of scale effects on the results. Values of δ_r were obtained by direct shear interface tests. Shear tests with sands, used in centrifuge tests, and steel, with and without welds, show that δ_r increases slightly for the welded surface. Shear tests with different sand samples and plate material, used in field tests, show that the grain size D_{50} did not influence δ_r for a given steel roughness. However, with larger D_{50} values the sand relative density had a greater influence on δ_r.

Comparison of measured and calculated values by the model are consistent with a mean value $Q_{h,\ measured}/Q_{h,\ predicted}$ of 0.98 and a coefficient of variation of 15.7 %. For the torque factor it was assumed that friction of the shaft was not significant, regarding the scale effects on the study. The presence of scale effects can be seen in Figure 8, which

is based on data from the literature, showing that the pile dimension significantly influences the torque factor.

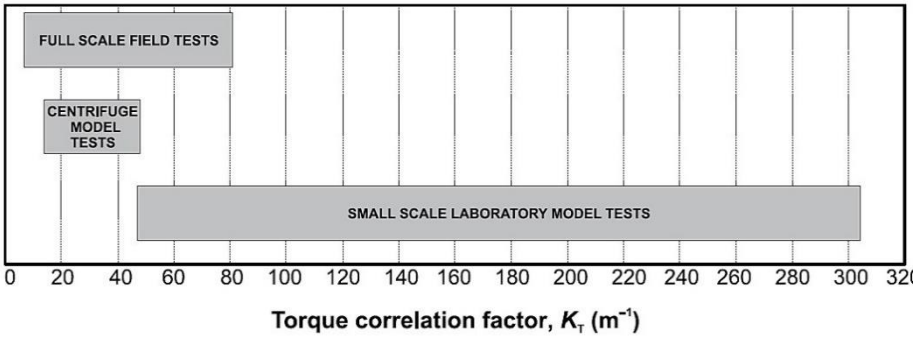

Figure 8: Comparison of measured torque factors (Tsuha and Aoki 2010)

Analyzing calculated torque factors $K_T = \frac{Q_h}{T_h}$ for the centrifuge along with the literature data showed that K_T decreased with an increase in sand relative density and helical plate diameter. Also, it decreased with an increase in δ_r and (or) an increase in d_c. Furthermore, K_T is not correlated with the number of helical blades.

2.2 Measurement of Interface Friction Angle

The interface friction angle is a major component in geotechnical engineering design and describes the shear interaction between soil and different construction material at the interface. To obtain interface friction angles, different types of shear tests can be performed in the laboratory. The calculation of the interface friction angle is based on the peak shear stress arising within the first millimeters of displacement. Also, after the

peak is reached, the shear stress reaches a constant residual shear stress for large displacements which is used to calculate the residual interface friction angle. For this study, large strains are assumed to arise during the helical pile installation process and therefore, residual interface friction angles are more applicable.

Uesugi and Kishida (1986) performed shear tests to investigate the frictional resistance at yield between sand and mild steel using the simple shear and the shear box method. They used different sands and varying steel surface roughness. Figure 9 shows the difference between these methods.

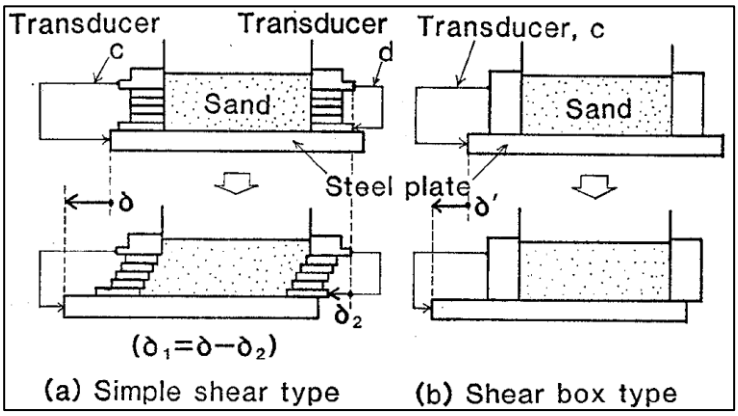

Figure 9: (a) Simple shear and (b) shear box method (Uesugi and Kishida 1986)

The simple shear uses a stack of rectangular aluminum frames as borders which changes the shape of the sand sample during the test, while the shear box uses a rigid steel frame which keeps the shape of the sample. They compared the resulting coefficient of friction (shear stress/normal stress) at yield and found no significant differences between the two methods, but they are lower compared to ring torsion shear tests. However, the displacement at yield was larger in the shear box.

Porcino et al. (2003) performed shear test using constant normal stiffness (CNS) and constant normal load (CNL) shear boxes to investigate the behavior of sand-solid interfaces. They used different silica sands and aluminum plates varying in surface roughness. They stated that a thin shear zone exists within the sand sample adjacent to the solid surface where shear strain occurs. This shear zone tends to dilate or contract during shear while the surrounding sand is the elastic confinement medium. For the CNL tests they found that the maximum shear stress and the displacement at this point increase with higher surface roughness and that the curves show a more pronounced softening behavior. The results from their study exhibited a contractive behavior in the beginning, which changed to dilative at larger displacements. For residual interface friction angles, they found in CNS tests, that they do not depend on relative sand density but on physical sand properties and surface roughness of the material tested. However, in the literature are also dependencies of the relative density reported. Porcino et. al (2003) explain this phenomenon by the collapsible structure inside the shear band which can cause loose sands to behave like a dense sand. This collapse is affected by the sand type and the sample preparation.

CHAPTER 3: DIRECT SHEAR TESTS

This chapter discusses the direct shear testing that was performed to obtain residual interface friction angles, which are used later as input to the analytical models. The equipment is described followed by the test results.

3.1 Direct Shear Testing Equipment

The testing was performed using a Shear Trac II manufactured by Geocomp and is shown in Figure 10.

Figure 10: Photograph of the Geocomp direct shear test device.

The shear box, shown in Figure 11, consists of two separate halves, which are moved against each other to create a horizontal shearing surface within the sand sample. Two nylon screws fix both parts initially together, while the four screws with springs are used to create a gap between the upper and lower halves of the shear box.

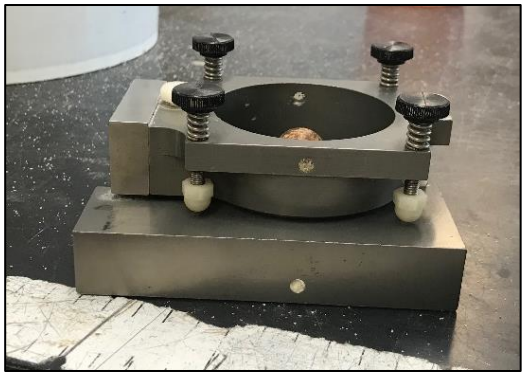

Figure 11: Photograph of the module for the sand sample

Vertical (normal) stresses are applied to the sample through a rigid top cap connected to a load cell at the top of the sample. Normal stresses can be applied to the sample as necessary to simulate different depths in the field. Horizontal (shear) stresses are applied to the soil by moving the lower half of the shear box while recording the reaction on the top half with a load cell. Both horizontal (shear) and vertical (normal) displacements are measured with a Linear Variable Differential Transformer (LVDT).

The sand used in this study was from a beach in Westerly, RI and its properties are summarized in Giampa & Bradshaw (2018) and in Table 2, where $\gamma_{max/min}$ is the max/min unit weight, e is the void ratio, D_{50} is the average grain size, and ϕ'_c is the critical state friction angle.

Table 2: Properties of Westerly beach sand

Parameter	Value
γ_{max} [kN/m^3]	18.10
γ_{min} [kN/m^3]	14.09
e_{max}	0.844
e_{min}	0.436
D_{50} [mm]	0.3
ϕ'_c [degrees]	32.2

The relative density was calculated for each test specimen using Equation 4, where γ is the measured unit weight of the test sample in kN/m^3.

(4) $$D_r = \frac{\frac{1}{\gamma_{min}} - \frac{1}{\gamma}}{\frac{1}{\gamma_{min}} - \frac{1}{\gamma_{max}}} \text{ x } 100\%$$

3.2 Direct Shear Testing

The equipment described above was used to perform direct shear tests on Westerly sand to refine the test procedures and to obtain the critical state friction angle of the soil. For the test runs, loose sand samples were dry pluviated, using a funnel with a 0.6 cm opening. The funnel was moved in circular pattern while maintaining a constant drop height of 6 to 7 cm to the sand surface. This process resulted in sand samples with relative densities of 4% to 8%. Some tests were conducted to quantify the amount of the friction between steel and steel of the shear box by running tests without any sand but by applying certain confining stresses to box.

Another test series was performed using the four spring-screws having nylon "feet" to create a gap to eliminate the steel-steel friction. The screws were not released to measure the friction between the nylon feet and the steel surface. The comparison of the results showed that the friction with and without the feet were approximately the same.

Next the spring-screws were used to create an initial gap and then retracted before shearing. The height of the gap was chosen to be the mean diameter (D_{50}) of the sand sample to prevent significant loss of sand from the shear box. The tests showed that the gap increased during shear and ended up with double the height of the beginning, with a significant loss of sand during the tests, which was reflected in the test results. In addition, the hole, created by removing the nylon fixing-screw, took a lot of sand as

soon as the top half shears over it, after approximately 8 mm. To solve this, the holes were pre-filled with sand.

The focus of the testing is on the measurement of the critical state interface friction angle of sand, which involves very large shear displacements that are representative of the installation of helical piles. Therefore, one way to accomplish this is to cycle the shear stress back and forth to bring the sand to the critical state. The results showed an increase of the residual friction force after every cycle what did not make sense. Also, there was significant sand loss. As a result, the cyclic approach was abandoned, and a monotonic approach was used as described next.

A series of direct shear tests were performed to characterize the residual friction angle of the test sand. The purpose of these tests was to provide a baseline for comparison to the residual interface friction angles discussed later on. The samples were pluviated using method funnel and then densified by hitting the shear box with a hammer on each side on both box halves. The densities varied between 19 and 28%. The specimen area decreases with shear displacement in the direct shear test. Therefore, the area was corrected using equation 4 (Olson and Lai 2004).

(5) $A = A_0 F$

[5a] $F = \frac{2}{\pi}\left\{\cos^{-1}\left(\frac{\Delta h}{D}\right) - \left(\frac{\Delta h}{D}\right)\sqrt{1-\left(\frac{\Delta h}{D}\right)^2}\right\}$,

where A is the corrected area, A_0 is the original area, F is the correction factor, Δh is the horizontal displacement, D is the diameter of the sample, and the arc-cosine is in radians.

The results of the direct shear tests on Westerly sand are shown in Figure 12. As shown in the figure, all curves show a peak shear stress, which gets better defined and shifts to the right with increasing confining stresses, as well as a more pronounced softening behavior after the peak. Also, the curve for 100 and 150 kPa reach a low point after the peak followed by a slight increase in shear stress with horizontal displacement, especially for 150 kPa. This is not consistent with critical state theory that indicates that the shear strength should remain constant at very large displacements. Therefore, failure was defined at the lowest value of the shear stress and the results are summarized in Table 3.

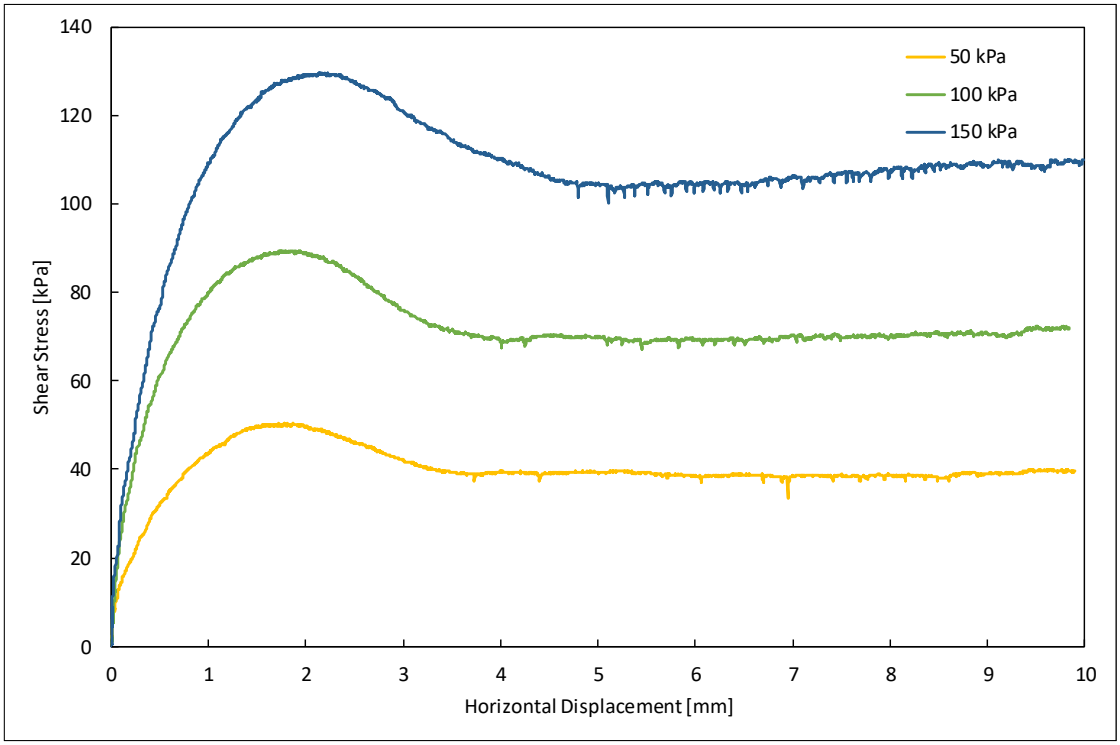

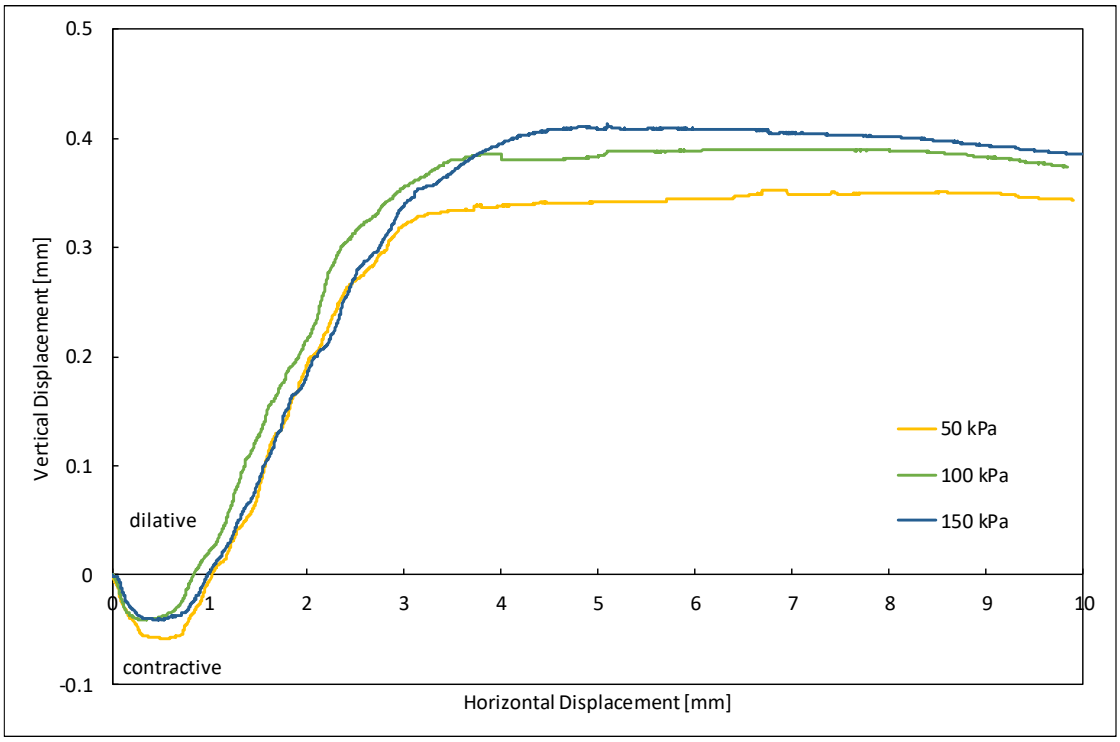

Figure 12: Shear Test results for direct shear tests on Westerly beach sand.

Table 3: Summary of residual shear stress results for the direct shear tests on sand

Confining Stress [kPa]	*Shear Stress at Failure (kPa)*
50	38
100	69
150	104

Regarding the volume change behavior, all curves tend to contract in the beginning and change to a dilative behavior after approximately 0.5 mm. The samples for 100 and 150 kPa confining stress show a slightly contractive behavior in the end while the 50 kPa sample almost shows no volume change indicating that the critical state was reached.

3.3 Interface Shear Testing

3.3.1 Equipment Modifications and Testing Procedures

Since the standard direct shear testing equipment is used to determine friction angles between sand and sand, modifications had to be made to the shear box to measure interface friction. To do this, the bottom half of the shear box was replaced with a metal plate on which different materials could be attached, as shown in Figure 13. The different materials were attached either with screws in each corner or with glue. The sand sample had a height of 24.5 mm and a diameter of 63.4 mm.

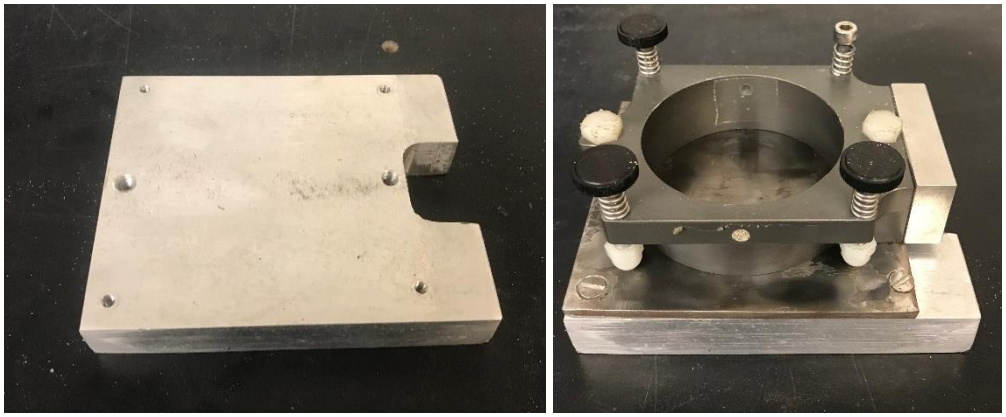

Figure 13: Photographs of the new base plate and the whole module

Dense samples were prepared to a constant relative density by air pluviation. Dense samples were used to minimize sample disturbance during sample preparation and

handling and to better identify when the residual shear conditions were reached in the test results.

To prepare the test specimens, a 2-mm diameter sieve was placed on top of the shear box and a small steel pipe, with a length of 132 mm, a diameter of 51 mm, and an attached plastic cap with three 2.5 mm holes, was used to pluviated the sand sample with a drop height of 20 cm to the sieve (Figure 14). The relative density that was achieved was around 65%, which correlates with the density used in the small-scale physical model tests on the helical piles. The materials used for the tests were a sheet of steel of the helical blade, a self-adhesive Teflon sheet, and a sheet of #60 grit sandpaper.

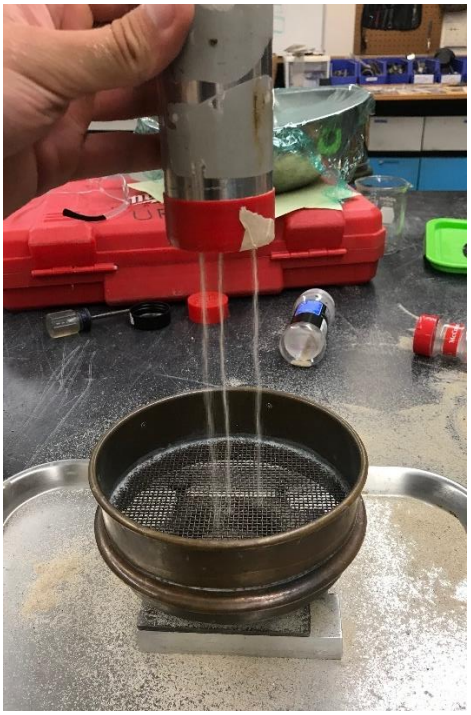

Figure 14: Photograph of the pluviation process

The following procedure was used for each of the interface shear tests. The software provided by Geocomp for Shear Trac II was used. Screen shots of the test parameters are provided in the Appendix.

1. The material was attached to the base plate.
2. The module halves were cleaned from sand particles and assembled by tightening the white fixing-screws.
3. The empty shear box was weighed.
4. The sand sample was pluviated in the described way.
5. The excess sand on top of the sample was scraped off and the shear box was cleaned from sand using a brush.
6. The shear box was weighed again to obtain the weight of the sand sample.
7. The shear box was placed and fixed in the box of the shearing device.
8. The top cap with the steel ball was placed on top of the sample and the cross bar was brought and fixed close to the steel ball. Adjustments of the position of the shear box were made to get it in line with the load cell. The horizontal level of the cross bar was checked with a water level.
9. All necessary options were set in the software program.
10. The test was started by position the platen and after, the pre-confining stress was applied.
11. The spring-screws were turned down until they slightly touched the base plate.
12. The distance between the top of the top half and the top of the bottom part was measured at each spring-screw using a caliper.
13. The white fixing-screws were released a little to create a gap.

14. The spring-screws were turned incrementally up to half of a full rotation while the mentioned distance was measured frequently, until a gap of around 0.3 mm was created.
15. The threaded rod of the horizontal load cell was fixed to the top half by tightening of the screw.
16. The white fixing-screws were removed, and the hole was filled up with sand and the excess sand was scraped off.
17. The spring-screws were released to eliminate any additional friction.
18. The wing screws used to fix the horizontal load cells were fixed carefully.
19. The shear phase was started.

Furthermore, the software provides the results of the shear test in form of a shear force in Newton. Hence, the residual shear force S_r needs to be converted to a shear stress τ_r by use of equation (6):

(6) $$\tau_r = \frac{S_r}{A},$$

where A is the cross-sectional area of the specimen (=0.003157 m^2). Table 4 provides a summary matrix of the tests that were performed as part of this study.

Table 4: Test matrix for interface shear tests

Confining stress /Material	15 kPa	50 kPa	100 kPa	150 kPa
Steel	3	3	3	3
Teflon	1	1	2	2
Sandpaper	2	1	2	1

3.3.2 Steel-Sand Interface Test Results

For the steel-sand interface tests, a sheet of steel, which was also used for the helical pile tests, was fixed to the base plate using flat screws (Figure 15). The steel surface was polished to clean it from possible debris. The sand was pluviated as described above to obtain dense sand samples. The relative densities for each test are summarized in Table 5.

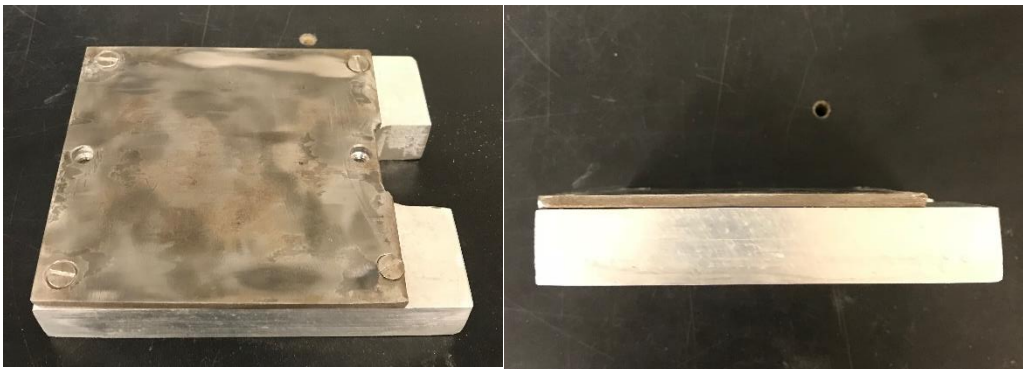

Figure 15: Photographs of the attached steel sheet

Table 5: Sample relative densities for the steel interface tests

Confining Stress [kPa]	*Relative Density (%)*		
	Steel #1	Steel #2	Steel #3
15	64.6	66.0	64.2
50	66.8	65.7	66.9
100	66.8	67.1	66.7
150	65.5	63.6	67.1

The first test series of tests was conducted with one test at each pre-confining stress. After this series, a Teflon sheet was attached for the Teflon tests and removed again to run another series of steel interface tests to validate the reproducibility. Before the second and third series, the steel sheet was polished and tests two and three for each

confining stress were conducted in succession because of significant variations between series one and two for most of the tests. Furthermore, it was observed that the gap, created in the beginning, increased slightly during the test from around 0.3 to 0.4 mm on the left side of the module, which is not fixed with a screw, especially for higher confining stresses.

The test results for a confining stress of 15 kPa are shown in Figure 16. As shown in the top of the figure, the shear data match very well. As expected, for low confining stresses, a peak is not well defined. The residual shear strength was reached right after the test was started and just some small variations are present. Overall, an average residual shear strength of 8 kPa for all curves can be read between 2 and 6 mm of horizontal displacement. The behavior of volume change is consistently dilative after it was very slightly contractive right in the beginning of the tests.

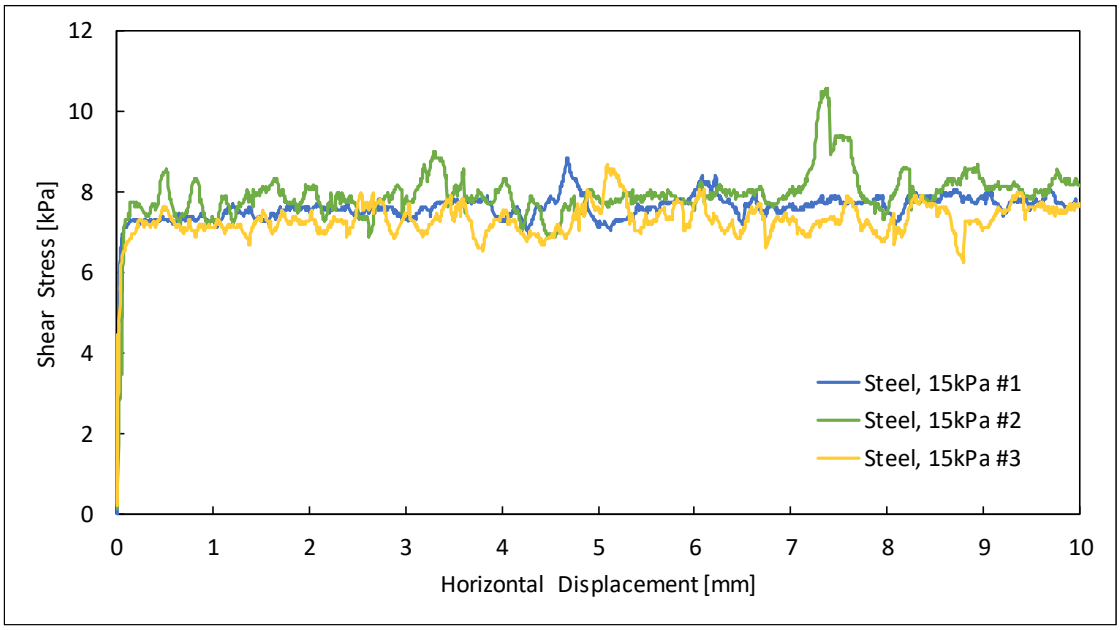

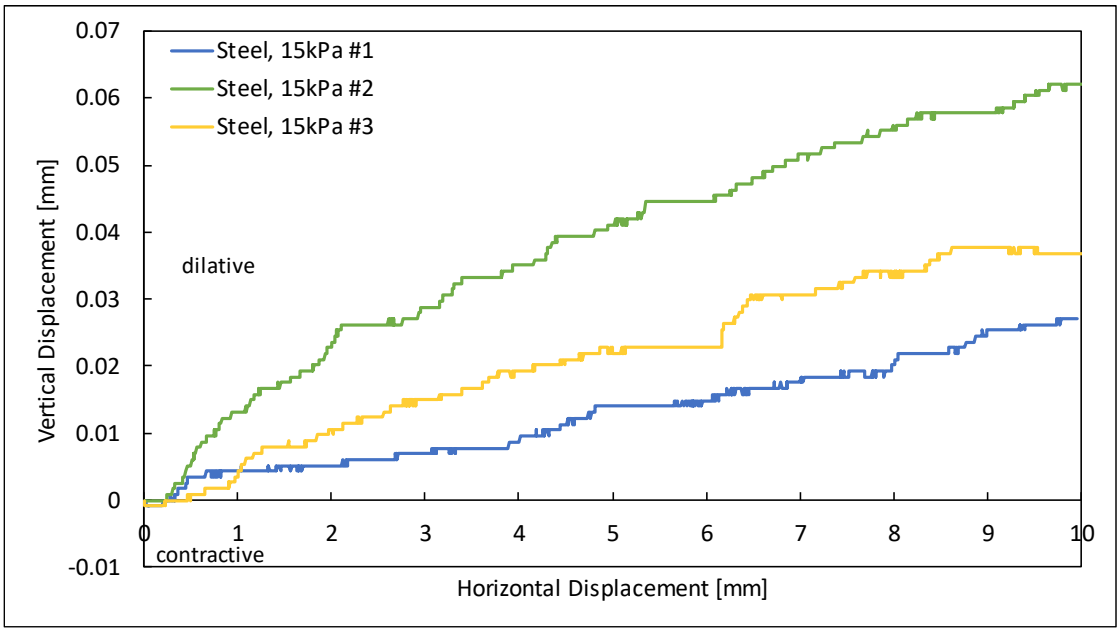

Figure 16: Interface shear test results for steel for 15 kPa

The results for the 50 kPa tests are plotted in Figure 17. The shear stress data were somewhat inconsistent for these tests. The average shear stresses at failure are 12, 17, and 20 kPa, respectively. Initially, all samples behaved slightly contractive and sample 1 kept on contracting for the rest of the test, while samples 2 and 3 changed to a dilative behavior.

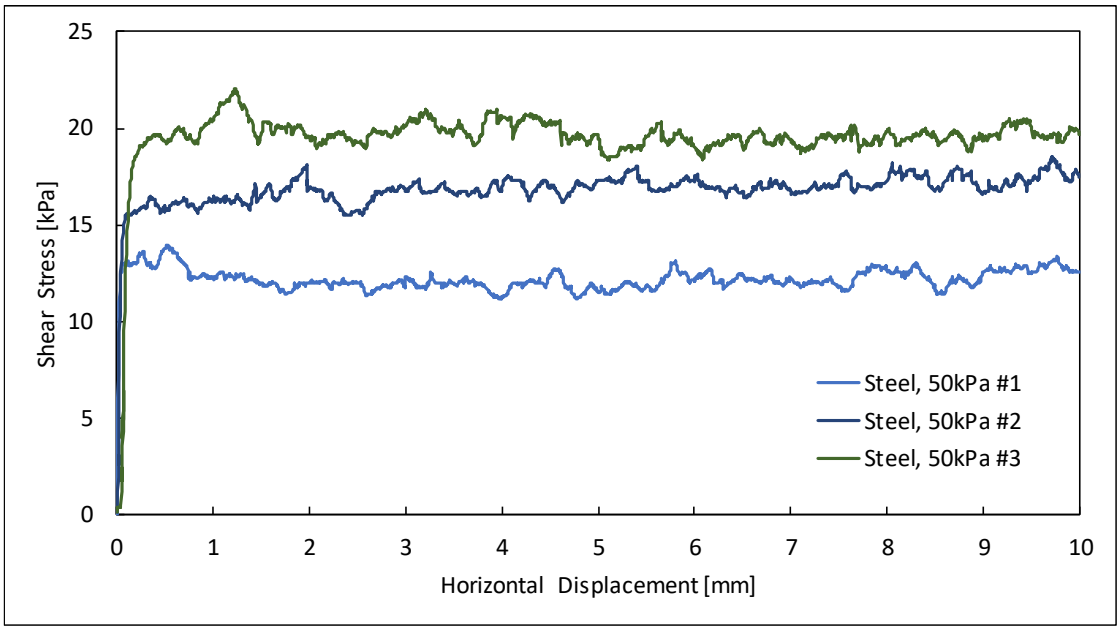

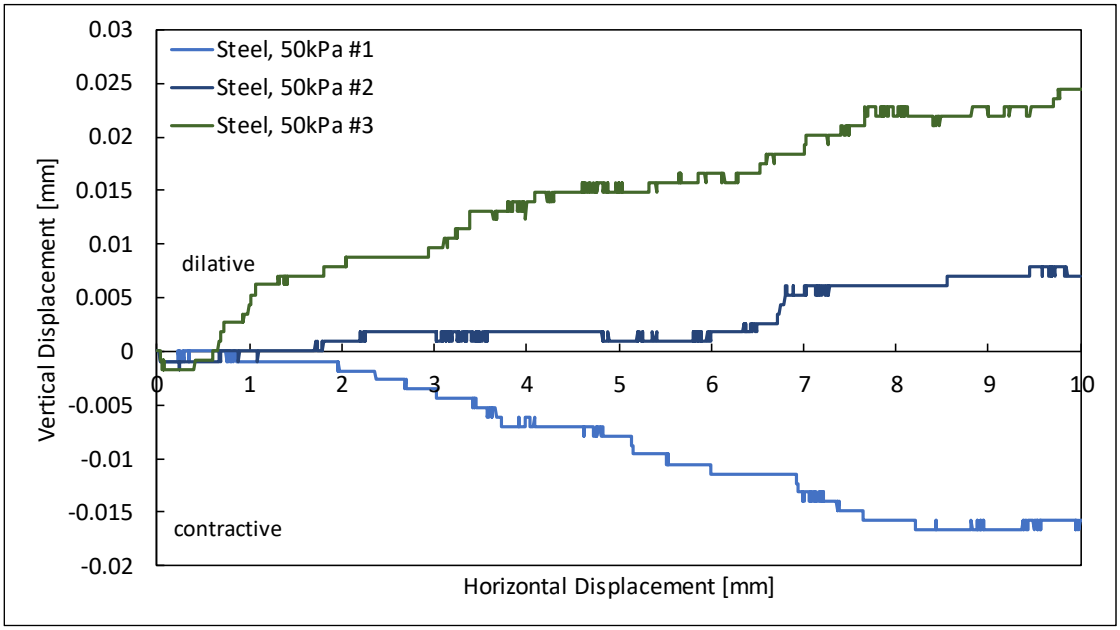

Figure 17: Shear Test results for steel for 50 kPa

The results of the shear tests for the 100 and 150 kPa tests are shown in Figure 18. The tests for 100 kPa and 150 kPa show similar results compared to the 50 kPa tests, showing both contractive and dilative volume change behavior. The first test for 150 kPa shows a unique volume change response. Initially it behaves contractive, then dilative, and contractive again within the first millimeter. The contractive behavior in the beginning was stronger and a well-defined peak in the shear stress developed. This suggests that this sample was probably very close to the critical state before shear. The shear stress in all tests softens after reaching a peak but then goes up again at a displacement of about 3 to 5 mm. Table 6 summarizes the interpreted residual shear stress for the steel interface shear tests.

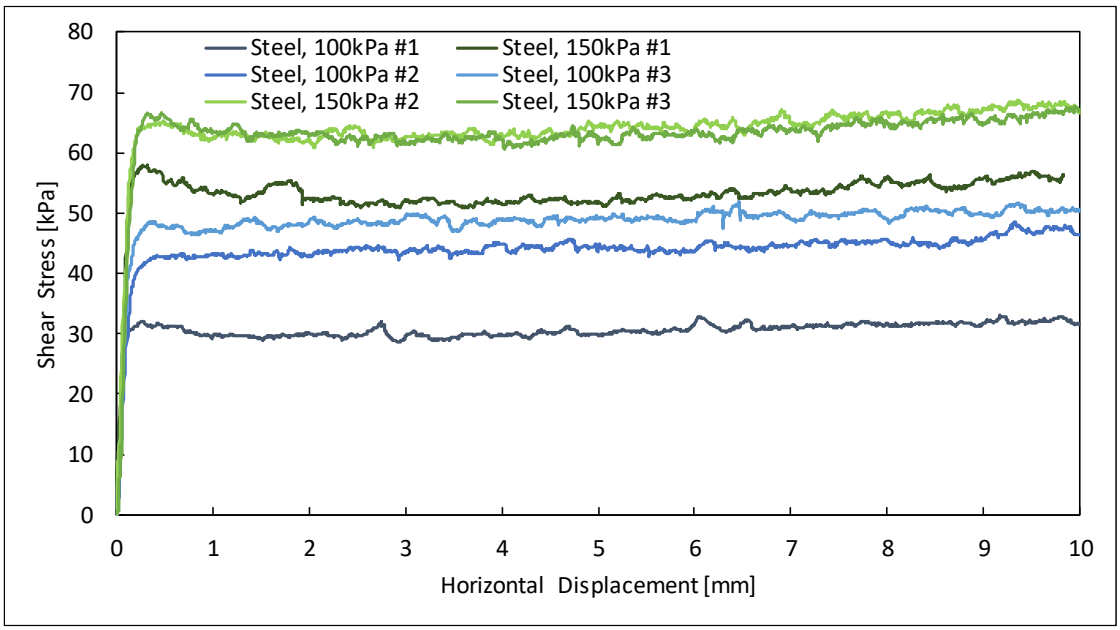

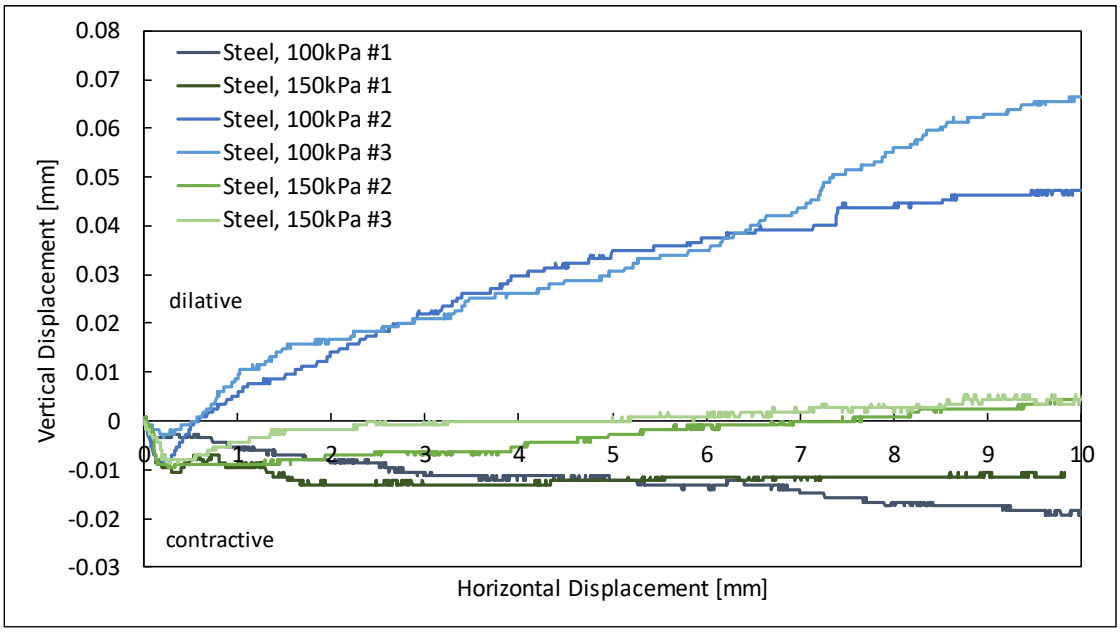

Figure 18: Shear Test results for steel for 100 and 150 kPa

The repeat tests showed significant variability in both shear and volume change response despite being prepared and tested in the same manner. However, the pluviation process may have resulted in significant variability in void ratio within the shear band, which could have affected the shear results. Even though the measured densities for all tests are almost the same, they are still an average property of the global sand sample, which can vary locally within the sample.

In the following, series 2 and 3 are considered only because of their reproducibility, but there was significant variability in the results. The increasing shear stress for higher confining stresses may be related to the increase of the gap, at which the tilting could cause a shift of the shearing angle. This shift could change the shearing movement to a

non-horizontal motion what means that shear process does not happen at the interface anymore. Also, this upward movement is not consistent with critical state theory in that the obtained shear stress slowly approaches a certain residual shear stress and stays constant. Therefore, failure was defined again at the lowest shear stress as summarized in Table 6.

Table 6: Summary of residual shear stress results for steel interface shear tests [kPa]

Confining Stress [kPa]	*Shear Stress at Failure (kPa)*		
	Steel #1	Steel #2	Steel #3
15	8	8	7
50	12	17	20
100	30	44	49
150	52	63	63

3.3.3 Teflon-Sand Interface Test Results

For the Teflon tests, a sheet of self-adhesive Teflon was attached to the top of the former used steel sheet (Figure 19).

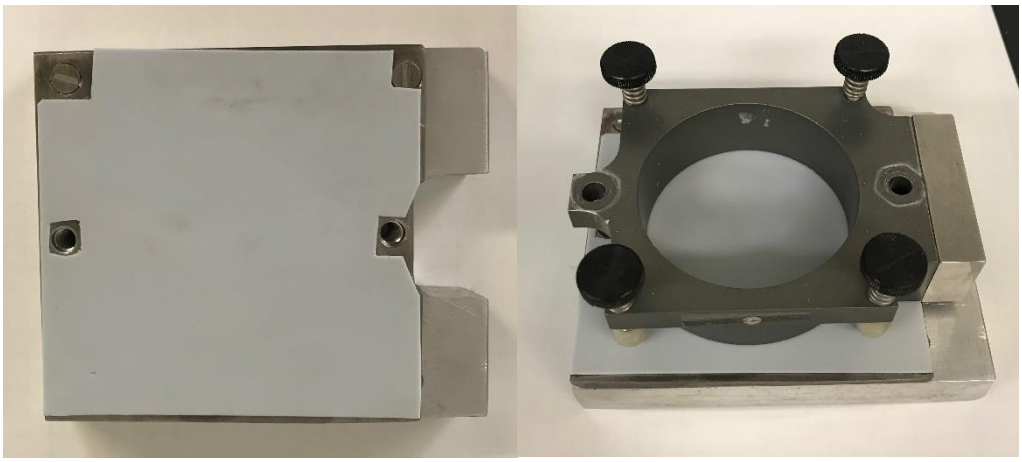

Figure 19: Photographs of the attached Teflon sheet

The relative densities, which are summarized in Table 7, are very consistent with a difference of only 1.87 % between the highest and the lowest one.

Table 7: Sample relative densities for the Teflon interface shear tests

Confining Stress [kPa]	*Relative Density (%)*	
	Teflon #1	Teflon #2
15	64.2	
50	66.8	
100	65.4	66.0
150	65.9	65.5

A first series of tests were performed, followed by two additional repeat tests to verify the reproducibility of the tests. After all tests, the Teflon sheet was observed and very small, almost non-visible, scratches were seen in direction of the shearing movement.

Figure 20 shows the results of all tests. It can be observed that the tests with a higher confining stress have a clearly defined peak, which moves to the right and gets better defined with an increase in confining stress. An explanation for the well-defined peaks could be that, due to the soft Teflon surface, sand particles got pushed into the Teflon what lead to an increase in peak shear strength. However, with continued displacement the sand grains rolled out of the grooves.

In general, all curves approach a critical state level at a displacement of 10 mm. For 15 kPa, there is almost no peak and the residual shear strength was reached right after the start of shear and stayed relatively constant with an increase in horizontal displacement.

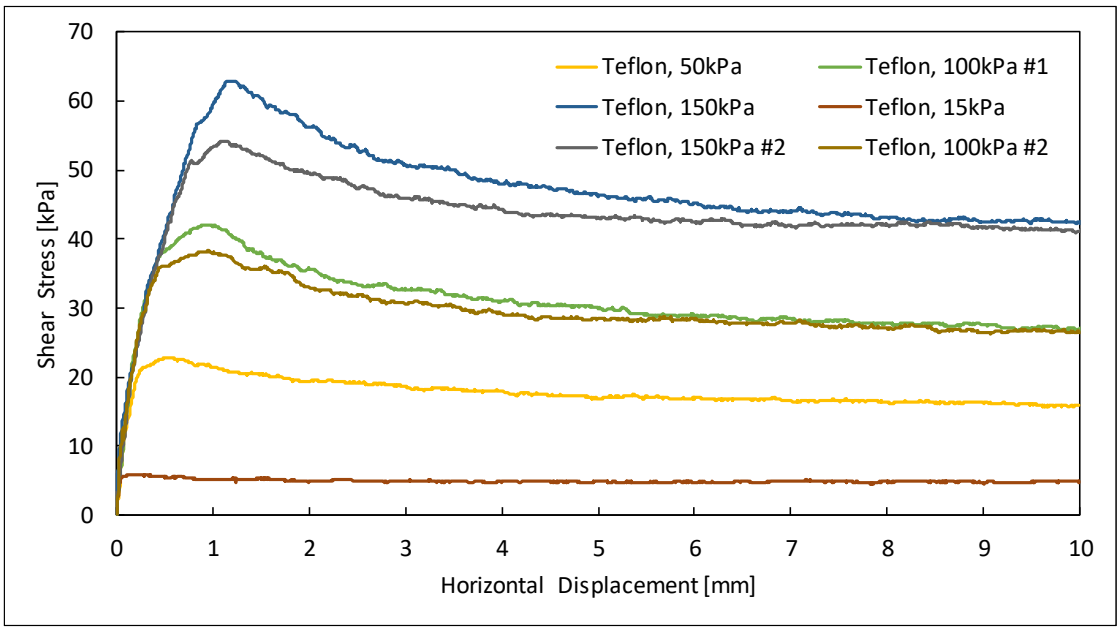

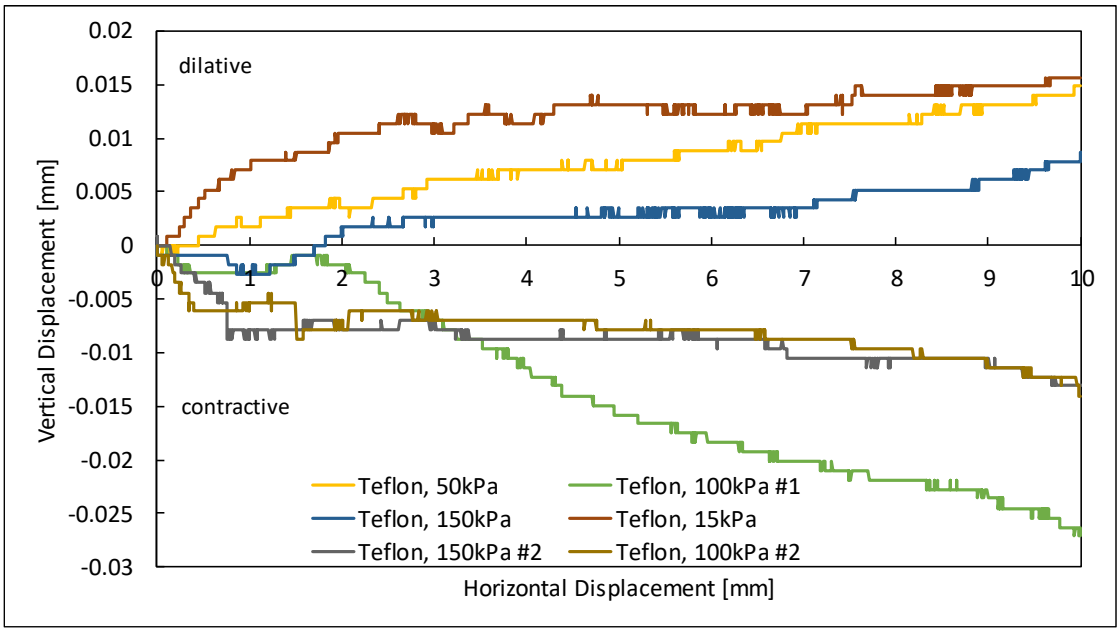

Figure 20: Shear Test results for Teflon

For the volume change the curves for 15 and 50 kPa show an ongoing dilative behavior. Both tests with an applied vertical load of 100 kPa show initially a contractive, then a dilative, and finally an ongoing contractive behavior after 2 mm. The first test was more dilative than the second test. The 150 kPa tests showed slightly different volume change behavior; one was loser and slightly contractive and the other was denser and slightly dilative. This suggests that the critical state void ratio at 150 kPa might lie between these two samples.

Since all curves seemed to approached a critical state at 10 mm, this is where failure was defined. The average residual shear strength for each test is summarized in Table 8. It increases with higher confining stresses and the values between both test series are almost the same.

Table 8: Summary of residual shear stress results for Teflon in [kPa]

Confining Stress [kPa]	*Shear Stress at Failure [kPa]*	
	Teflon #1	Teflon #2
15	5	
50	16	
100	27	27
150	42	41

3.3.4 Sandpaper-Sand Interface Test Results

For the rough surface tests, a sheet of #60 grit sandpaper was glued on top of the steel plate (Figure 21).

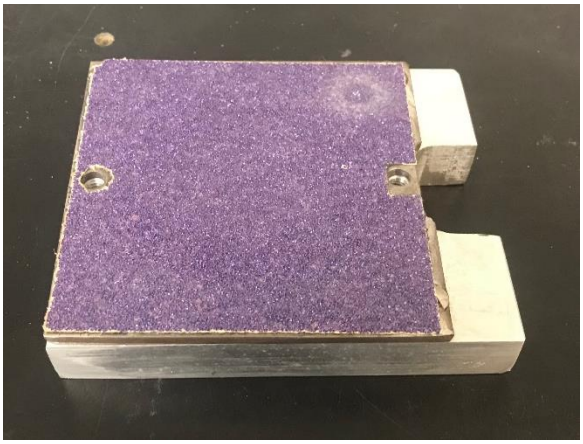

Figure 21: Photograph of the attached sandpaper sheet

The densities for all tests are summarized in Table 9. There is no significant variation, but the densities are approximately 7 % higher compared to the steel and Teflon tests, despite that the same pluviation process was used.

Table 9: Sample relative densities for the sandpaper interface shear tests

Confining Stress [kPa]	*Relative Density (%)*

	Sandpaper #1	Sandpaper #2
15	72.5	71.6
50	72.5	
100	72.7	70.2
150	71.5	

Right before the actual shearing process, the gap between the shear box increased significantly during the test, from 0.4 up to more than 1 mm. Since it was difficult to measure the height of the gap because of the rough surface, a piece of paper was used to check the gap. It was observed that sand particles got stuck on the sandpaper surface right after the sand sample sheared over it because of its roughness. Before each new test, the sandpaper surface was carefully cleaned with a brush to remove all sand particles. The test for 15 and 100 kPa were performed twice to validate the reproducibility of the tests.

Figure 22 shows the results of the sandpaper interface tests.

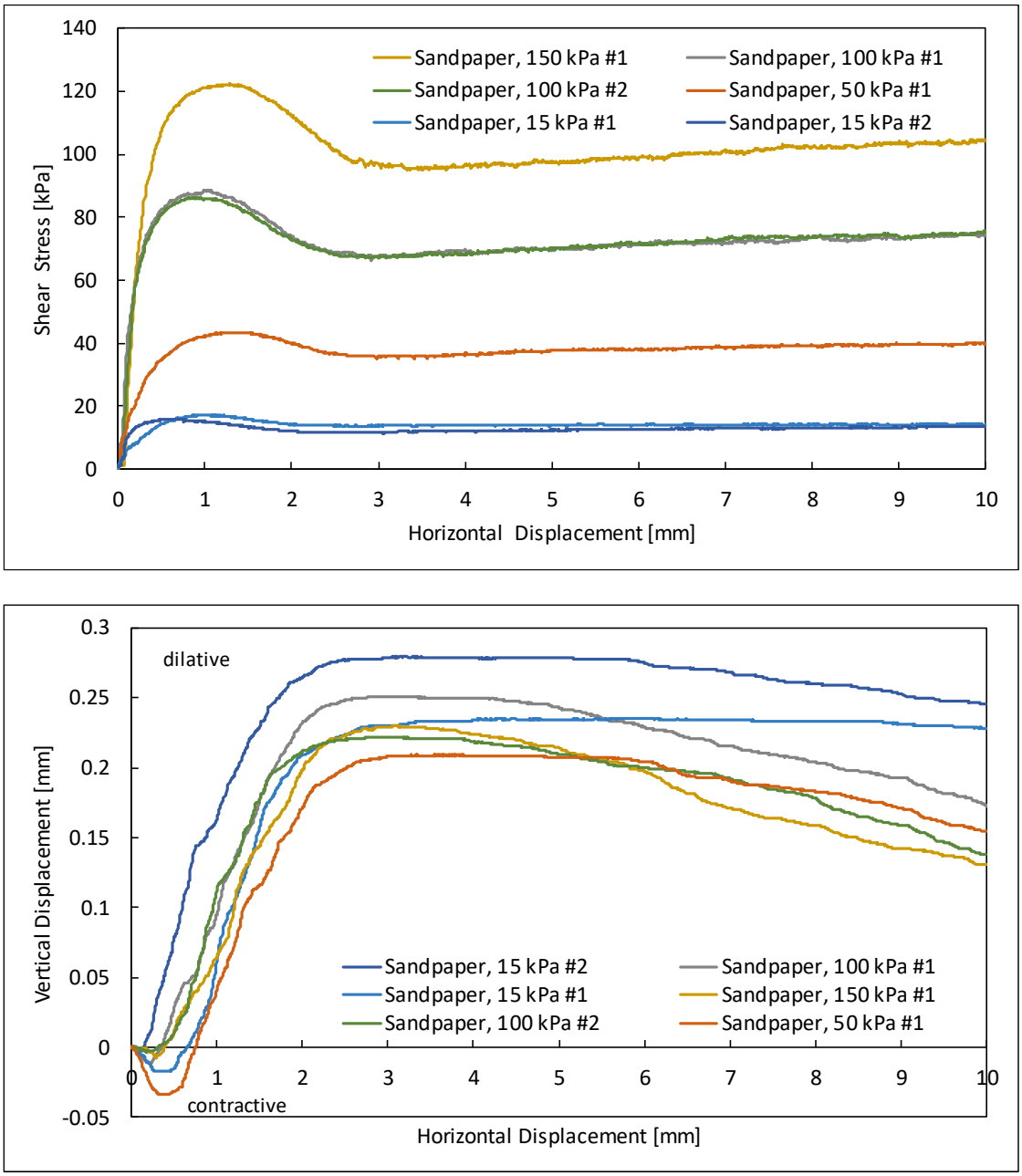

Figure 22: Shear Test results for sandpaper

The peak is more gradual and shifts to the right at higher confining stresses. In general, the shear stress increases with an increase in confining stress. After the peak was reached the shear stress decreases to a low point at about 3 mm of displacement followed

by a slight increase. For the 15 kPa test this phenomenon is not observable, since they reach a low point after the peak which stays almost constant with horizontal displacement. The second validation test series show almost the same results, especially for the 100 kPa tests, which match very well. For the second 15 kPa test, the shear force increases slower initially and the peak value was reached later. This smooth increase can also be observed for the 50 kPa test, in contrast to the other tests which show an initial steep increase.

The volume change behaves similar for all tests. The samples show an initially contractive behavior, followed by dilation after about 0.5 mm. At larger displacements of about 4 mm the volume change shows a tendency toward contraction. As compared to the other interface test results, the samples showed orders of magnitude higher volume changes. This may be due to the sand particles being pushed over the asperities of the sandpaper surface.

The increase in shear stress at large displacements could be explained by the rotation of the top cap and shift of the failure plane away from the interface. It seems like the size of the gap also controls the slope of the increase. Since this behavior is not consistent with critical state theory, failure was defined at the lowest shear stress, as summarized in Table 10.

Table 10: Summary of residual shear stress results for sandpaper interface shear tests

Confining Stress [kPa]	*Shear Stress at Failure (kPa)*	
	Sandpaper #1	Sandpaper #2
15	14	12
50	36	
100	67	67
150	96	

3.3.5 Calculation of Residual Interface Friction Angle

Figure 23 shows a plot of residual shear stress at failure vs. normal stress at failure, whereas each data point represents one test. The steel test series 1 was not included in the calculation of friction angle, as they are believed to be outliers.

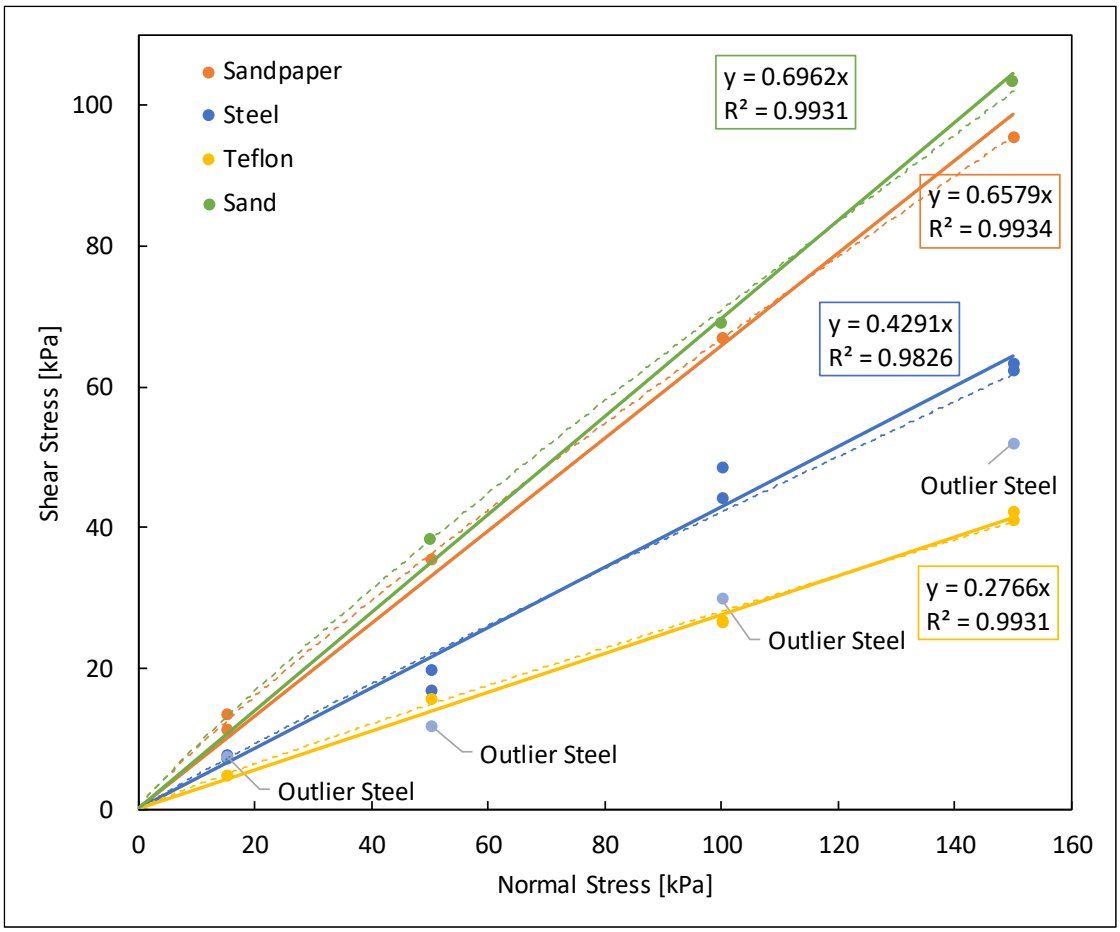

Figure 23: Normal stress vs. shear stress

A linear trendline was fit through the different test series from which the interface friction angle was determined and summarized in Table 11. A curved failure envelope was also fit to the data in Figure 26 shown as dashed lines. As shown in Table 11, the residual friction angle for the sand on sand is the highest, followed by the sandpaper, the plain steel, and the smooth Teflon surface, which is the lowest. The data points for

the Teflon and sandpaper surface match the average trend line the best and show only small variations, in contrast to the steel which show greater variances, especially for the 50 and 100 kPa tests.

Table 11: Summary of calculated residual interface friction angles

	Residual interface friction angle, $\delta_{r\,[°]}$
Teflon-sand	15.5
Steel-sand	23.2
Sandpaper-sand	33.3
Sand-sand	34.8

As expected, the residual interface friction angle increases with the increase in surface roughness. The similarity between the linear and non-linear failure envelopes suggest that there is little effect of confining pressure on the residual friction angle. This is consistent with critical state theory that suggests that residual interface friction angles should be independent of confining pressure and density. Also, the friction angles of the sand on sand and the sandpaper tests are in the same range, which is reasonable because the sandpaper surface consists essentially of a fixed surface of sand particles. Also, the tests on steel are consistent with common rules of thumb that suggest that the interface friction angle should be approximately 3/4 times the friction angle of the soil (Ghaly and Hanna 1991).

CHAPTER 4: ANALYTICAL MODELING

This chapter presents the analytical modeling of the physical model tests that were performed on helical piles as described in Zuelke (2018).

4.1 Summary of Helical Pile Test Data

A series of installation and pullout tests for helical piles were conducted and measurements of the required installation torque and the pullout resistance were taken. Different modifications were made to the helical anchor to see how it affected the installation forces and the pullout capacity. Details of the anchor modifications and testing results are presented in Zuelke (2018). Two of the anchor modifications included attaching a Teflon coating and sandpaper to the blade, respectively. A third modification was made to simulate "jetting" whereby sand was vacuumed out of the anchor shaft during installation. The helical piles were installed and tested in both loose and dense sand. The properties of the helical piles are shown in Table 12, the test sand properties are in Table 13, and the test results are in Table 14. The following three-letter abbreviation is used to describe each test. The first letter L=loose or D=dense, the second P=plain (steel), R=rough (sandpaper), S=smooth (Teflon), or J=jetted, the third letter O=open ended, or C=closed ended, followed by the test number. LPC1 would be used for an anchor installed in loose sand, having just the steel as the blade, with a closed end installation.

Table 12: Properties of the helical piles used for the tests

Property	*Value*
Installation depth [cm]	115
Shaft outer diameter [cm]	4.57
Shaft inner diameter [cm]	4.27
Blade diameter [cm]	12.7
Pitch [cm]	1.8
Blade thickness steel [cm]	0.38
Blade thickness Teflon [cm]	0.51
Blade thickness sandpaper [cm]	0.47
Res. Int. friction angle steel [°]	23.2
Res. Int. friction angle sandpaper [°]	33.3
Res. Int. friction angle Teflon [°]	15.5

Table 13: Properties of the sand used for the tests

Property	*Loose*	*Dense*
Unit weight, γ [kN/m^3]	15.0	16.5
Relative density (model), D_r [%]	27	65
Relative density (prototype), Dr [%]	65	99
Peak friction angle, Φ [°]	37.5	42.7
Average grain size, D_{50} [mm]	0.3	0.3

The peak friction angles presented in Table 12 were calculated using an empirical equation developed by Bradshaw & Giampa (2018). The equation was used to interpret the peak friction angle in the physical model experiments based on the measured relative density and estimated mean confining pressure at failure. The equations and calculations are provided in the Appendix.

The size of the model pile had to be scaled 1/5 from the original anchor by A. B. Chance. The confining stresses within the soil of a small-scale model will be lower than in the prototype at 1g. Since dilation in a soil with constant void ratio increases with decreasing confining pressures, model soils will behave more dilative. Hence, the density of the model sand must be made looser to behave like the prototype sand. At 1/5 scale the relative density of the model of 27% will behave as a prototype pile in a soil having a relative density of 65%. A relative density of 65% in the model will behave as a soil having a relative density of 100% in the field.

Table 14: Results of conducted helical pile installation tests

Pile	*Crowd Force, F_c [N]*	*Average Torque, T [Nm]*	*Pullout Load, Q [N]*	*Torque Factor, K_T [m^{-1}]*
Loose (D_r= 27 %)				
LPC1 (steel)	680	27	1800	64
LRC1 (sandpaper)	680	32	2000	61
LSC1 (Teflon)	680	23	1450	61
LSC2 (Teflon)	680	19	1450	75
LJO1 (“jetted”)	680	18	1250	65
Dense (D_r= 65 %)				
DPC1 (steel)	680	204	8700	42
DPC2 (steel)	2550	207	7500	36
DRC1 (sandpaper)*	2550	210	8550	40
DSC1 (Teflon)*	2550	181	9100	50
DJO1 (“jetted”)	2550	83	5800	69

*Attached sheets ripped off during installation process, hence the results will not be considered for further calculations.

4.2 Perko: Energy Method

Perko (2001) derived a model to predict the torque factor, based on the energy needed both to install and pull out the anchor. Perko (2001) used published data from the literature to test the model and made several assumptions for input variables. As part of this study, calculations were made for the data presented in Perko (2001) but the published results could not be replicated due to uncertainties in the input data.

4.2.1 Calculations

The model uses equation 7 to predict uplift capacities.

(7) $$Q = \frac{12d(2\pi T + Fp)[r^2 + \sum_m (R_m^2 - r^2)]}{3[2r^3 p + \sum_n (R_n^2 - r^2) t_n^2] + 16\pi\alpha[3r^3\lambda + \sum_m (R_m^3 - r^3) t_m]},$$

where d=vertical displacement to failure, T=installation torque, F=downward force exerted during installation (i.e. crowd), p=pitch per revolution, R_m=radius of m^{th} helical blade, r=radius hub, R_n=radius of n^{th} cutting blade, t_n=thickness of n^{th} cutting blade, α=ratio of side shear stress to penetration resistance, λ=length of hub experiencing side friction, and t_m=thickness of m^{th} helical blade.

To apply the model to the test data, a variety of assumptions had to be made. λ represents the length of hub experiencing side friction, and this should be equal the pitch of the blade. Perko (2001) verified this assumption by stating that this choice matched the measured results best. The ratio of side shear stress to penetration resistance α was set to 0.6 and is assumed to be proportional, as stated in Perko (2001). Also, the model requires the displacement at failure during the pullout test as an input, which was

assumed to be the displacement at the peak value for the pullout capacity. The measured values of displacement to peak capacity are presented in Table 15.

Table 15: Measured Values for the vertical displacement at failure during loading

Vertical displacement at failure, d [cm]					
Loose	**Steel**	**Sandpaper**	**Teflon 1**	**Teflon 2**	**Jetted**
	4.1	3.0	5.8	4.5	7.3
Dense	**Steel 1**	**Steel 2**	**Sandpaper**	**Teflon**	**Jetted**
	3.5	2.5	2.9	2.2	4.5

The remaining input parameters can be found in Chapter 4.1, whereas the downward force exerted during installation equals the crowd force. Equation 8 was used to calculate the predicted the uplift capacity and the division by the measured installation torque results in the predicted torque factor K_T, which is then compare to the measured value in the physical model tests.

4.2.2 Results and Discussion

Figure 24 presents the results and compares the predicted to the measured torque factor. The black solid line represents a 1:1 ratio indicating perfect model prediction. Overall, the model overpredicts the torque factor in both loose and dense sand. It can be observed that the data points spread widely, especially for the loose tests, which are off by factor 1.4 to 3.8. For the Teflon tests, the factors are 1.7 and 2.65. The sandpaper and Teflon tests in dense sand are not considered because the attached sheets on the helical surface ripped off during the installation process, and hence, no accurate statements can be made.

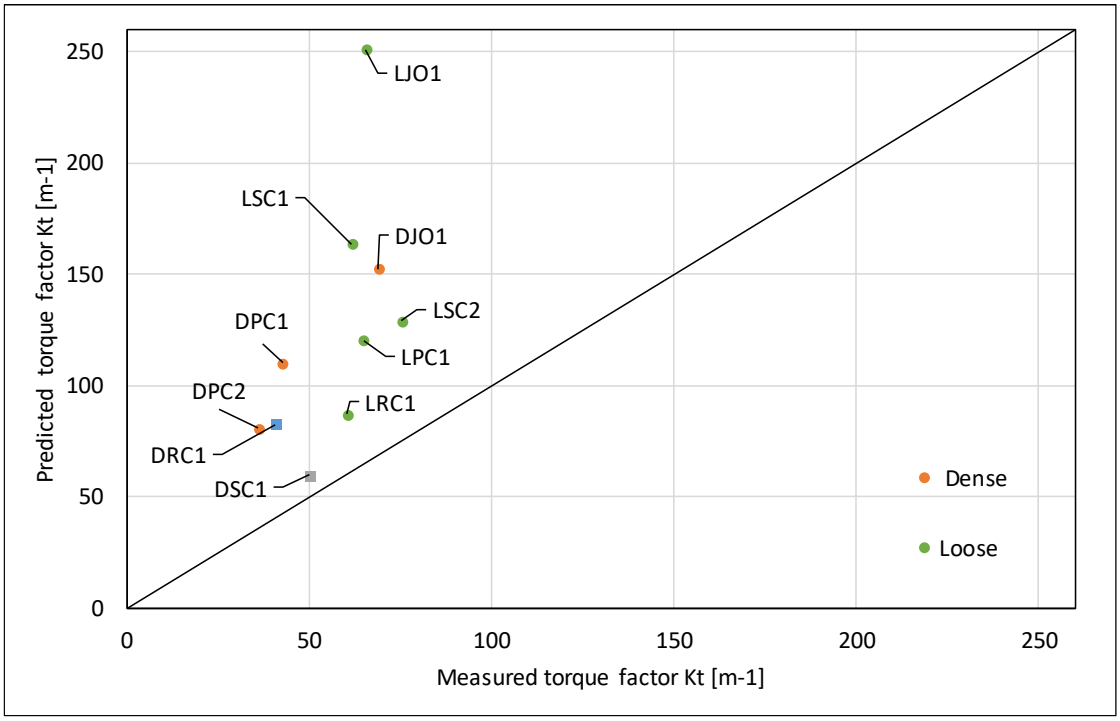

Figure 24: Comparison between measured and predicted torque factor K_T

The model results are very sensitive to changes in the vertical displacement parameter (d), which varied widely for the tests in this study. Also, the chosen values for α and λ are not proven to be right, and they can change the results significantly, as well. For example, λ (length hub experiencing side friction) was chosen to be one time the pitch height because it matched the results best, but this length could be significantly higher. Doubling of this value from 1.8 to 3.6 cm (just 1.8cm more for an overall length of 115cm of the pile), already decreases the torque factor by 25%. Also, an increase of 10% for α, results in a decrease of the torque factor by 10%.

Based on these uncertainties, the observed trend for the overprediction of the dense test results cannot be verified. Conceptually the use of energy concepts is valid because it captures the major components of resistance. However, the necessary input data are either very sensitive to changes or cannot be chosen accurately and would need to be investigated further.

4.3 Ghaly & Hanna: Torque Equations

Ghaly and Hanna (1991) investigated the interaction between soil and pile and put a focus of the development of a model, which predicts the required torque to install a helical anchor. Based on a free body diagram of the forces on the anchor, they came up with seven different torque equations which sum gives the overall required installation torque. The proposed model does not provide a direct correlation between required installation torque and uplift capacity, but they did provide an equation which correlates the calculated torque (matching the measured torques) to measured uplift capacity values of their conducted tests.

As a first step, a calculation spreadsheet was set up to replicate the data provided by Ghaly & Hanna (1991). The obtained results differed slightly from their results, but no calculation errors were found. Also, no published erratum was found. Since the differences were very small and the results were almost reproduced, the model was applied to the anchor test data in this study.

4.3.1 Calculations

The torque equations developed by Ghaly and Hanna (1991) are shown below,

[8a] $T_1 = 0.5\gamma H^2 \cos\delta\, K_p' K_f (\pi D)(\frac{D}{2})$

[8b] $T_2 = 0.5\gamma H^2 \sin\delta\, K_p' \tan(\delta + \psi)\, (\pi D)(\frac{D}{2})$

[8c] $T_3 = 0.5\gamma H^2 \sin\Phi\, K_p' \tan(\delta + \psi)\, (\pi B)(\frac{B}{2})$

[8d] $T_4 = \gamma H \sin\delta\, K_A A_t \tan(\delta + \psi)\, [\frac{B+B_0}{4}]$

[8e] $T_5 = \gamma H \sin\delta\, K_p A_b \tan(\delta + \psi)\, [\frac{B+B_0}{4}]$

[8f] $T_6 = \frac{F(B-B_0)^2}{8}$

[8g] $T_7 = \gamma H K_p K_f (\pi B)(\frac{B}{2})t$

where T_1 is the resisting moment on the shaft, T_2 and T_3 are resisting moments on the blade, T_4 is the resisting moment acting on the upper surface of the blade due to the active earth pressure, T_5 is the resisting moment acting on the lower surface of the blade due to active earth pressure, T_6 is the resisting moment owing to the bearing force acting on the height of the screw pitch, and T_7 is the resisting moment due to passive resistance on the leading edge of the screw blade. The Detailed derivations of the equations are presented in Ghaly and Hanna (1991).

For their model, Ghaly & Hanna (1991) used a rule thumb to calculate the interface friction angle δ assuming it is ¾ of the peak friction angle of the sand sample. In this study, the interface friction angle was measured directly in the laboratory (Chapter 3) and thus is used in the calculations. Since the pile is subjected to large displacements during the installation process, the residual interface friction angle δ_r, obtained from the shear tests was used. Also, depending on the pile tests, two different values of δ_r were

used. For T_1, which is due to the shaft resistance, the steel-sand interface friction angle was used, while for T_2 either the steel-sand or Teflon-sand interface friction was used depending on the anchor.

The first step consists of the application of the torque equations to obtain the required installation torque. The torque data is then used as an input for the following correlation to predict the uplift capacity of the pile (Ghaly and Hanna 1991):

(9) $$\left[\frac{Q_u}{\gamma AH}\right] = 2\left[\frac{T}{\gamma AHp}\right]^{1.1},$$

where Q_u is the uplift capacity, A is the anchor's surface area, H is the installation depth, and p is the pitch of the helix. After, the torque factor K_t can be calculated by dividing Q_u/T. Furthermore, equation 9 was used separately from the proposed torque equations. Therefore, the available data from the own piles tests is used as an input to see if reasonable agreement can be obtained.

4.3.2 Results and Discussion

Figure 25 shows a comparison between measured and predicted installation torque. Since the main goal of the proposed model is to predict the installation torque, these results are presented in addition. The solid black line represents a ratio of 1:1. For the loose tests, the models tend to overpredict by a factor between 4 and 7.5. Both predictions for the Teflon tests are close together and have a factor of 4.1 and 4.9. The torque for the steel and jetting tests are predicted with the same value.

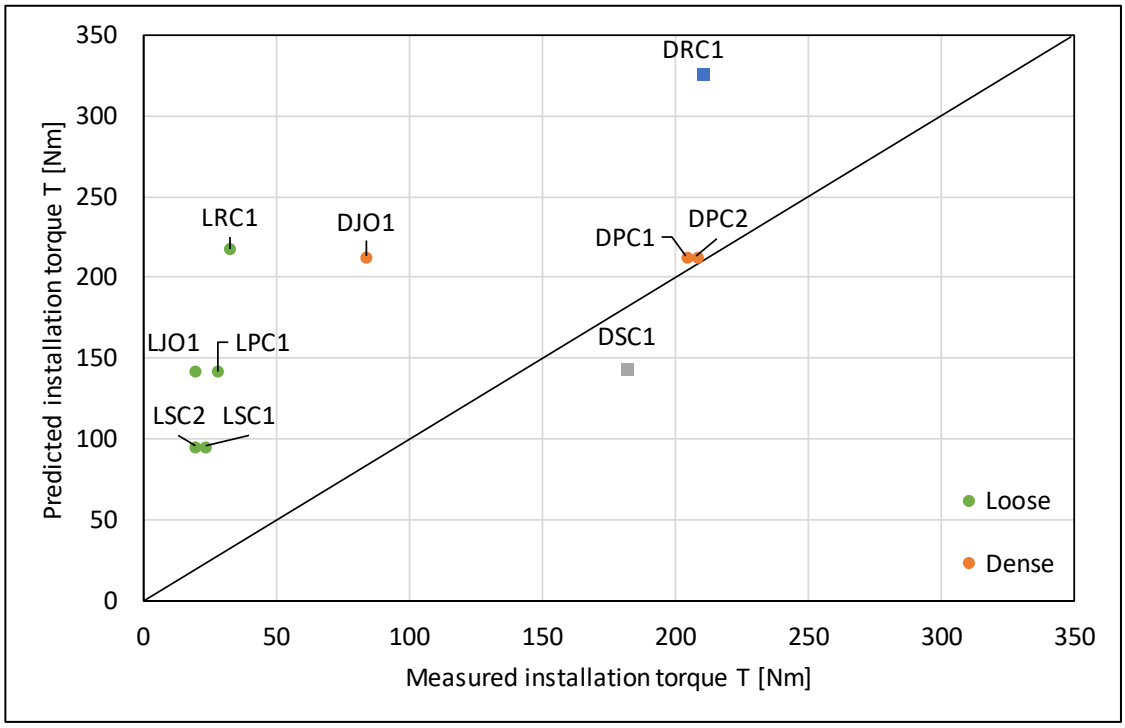

Figure 25: Comparison between measured and predicted installation torque using the Ghaly and Hanna (1991) model.

For the dense series, the sandpaper and Teflon tests were not considered because the sheets ripped off during the installation process. The predictions for both steel tests

match the measured values almost exactly. In contrast, the jetted test is overpredicted and has the same value as the steel predictions.

The predicted torque values were then used as an input for Equation 9 to calculate the predicted uplift capacity and to compare them with the measured capacities. The results are shown in Figure 26.

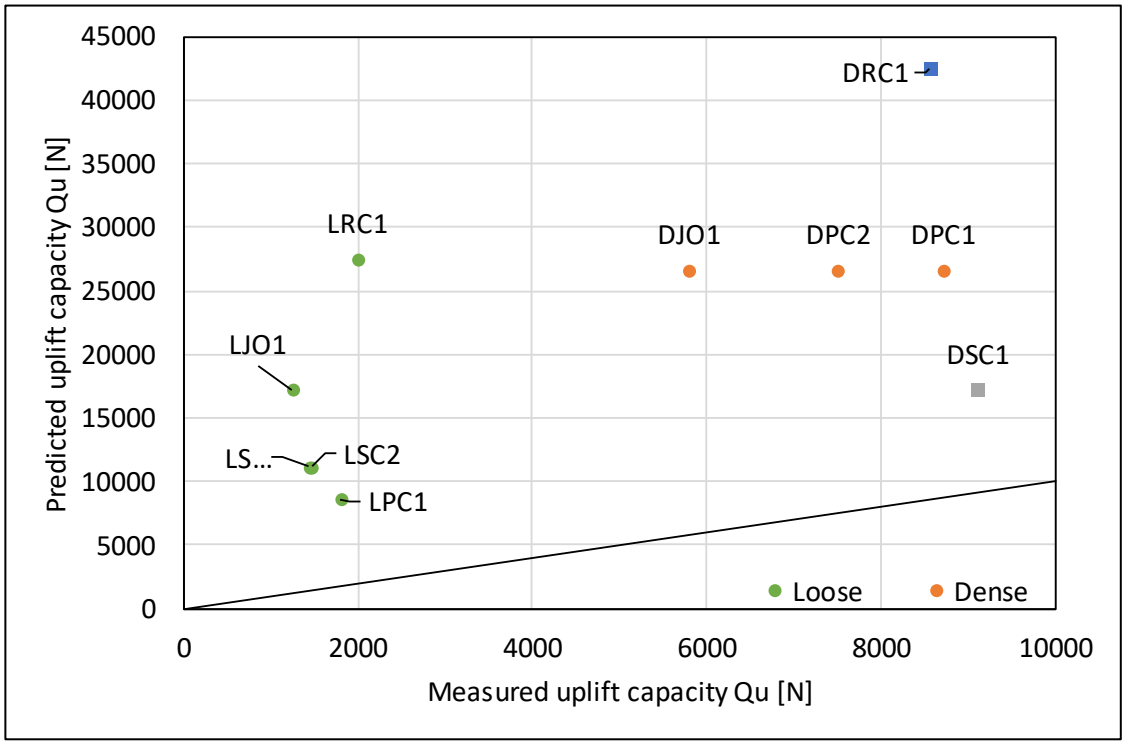

Figure 26: Comparison between measured and predicted uplift capacity using the Ghaly and Hanna (1991) model.

The black line represents a 1:1 ratio, as well. It can be observed, that equation 8 tends to heavily overpredict the uplift capacity, especially for the loose tests. The dense steels capacities are overpredicted by a factor of 3 to 3.55 and the jetted one by 4.61. The loose

tests vary significantly by factors between 7.7 for Teflon and 13.8 for sandpaper what gives capacities around 10 to 27 instead of 1 to 2 kN.

Furthermore, equation 9 was used independently from the proposed torque calculation and the measured torque data is used as an input to predict the uplift capacity. Hence, the torque factor was calculated and compared to the measured one. The results are shown in Figure 27.

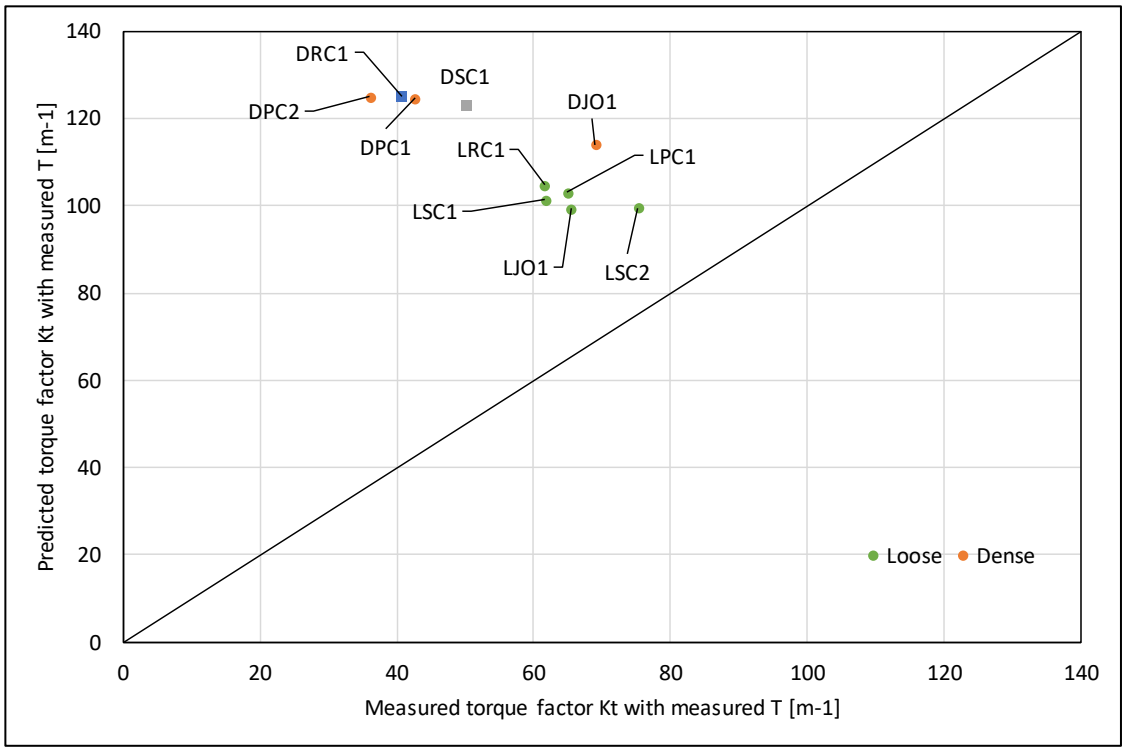

Figure 27: Comparison between measured and predicted torque factor K_T by use of measured torque values

Similar results are observed. The model tends to overprediction and the loose tests are off by 50 % on average. The dense steel tests are overpredicted by a similar factor as before, but the predictions between the dense tests do not lead to the same results.

Figure 28 shows a plot of the proposed non-dimensional equation 10 of Ghaly and Hanna (1991) and the own measured data points and is given to obtain a better comparison to their results. The dimensionless factors for the uplift capacity and the torque are calculated by equations 10 and 11

(10) $N_{qu} = \frac{Q_u}{\gamma AH}$,

(11) $F_t = \frac{F_t}{\gamma AHp}$,

where γ is the unit weight of the sand, A is the anchors surface area, H is the installation depth, and p is the pitch.

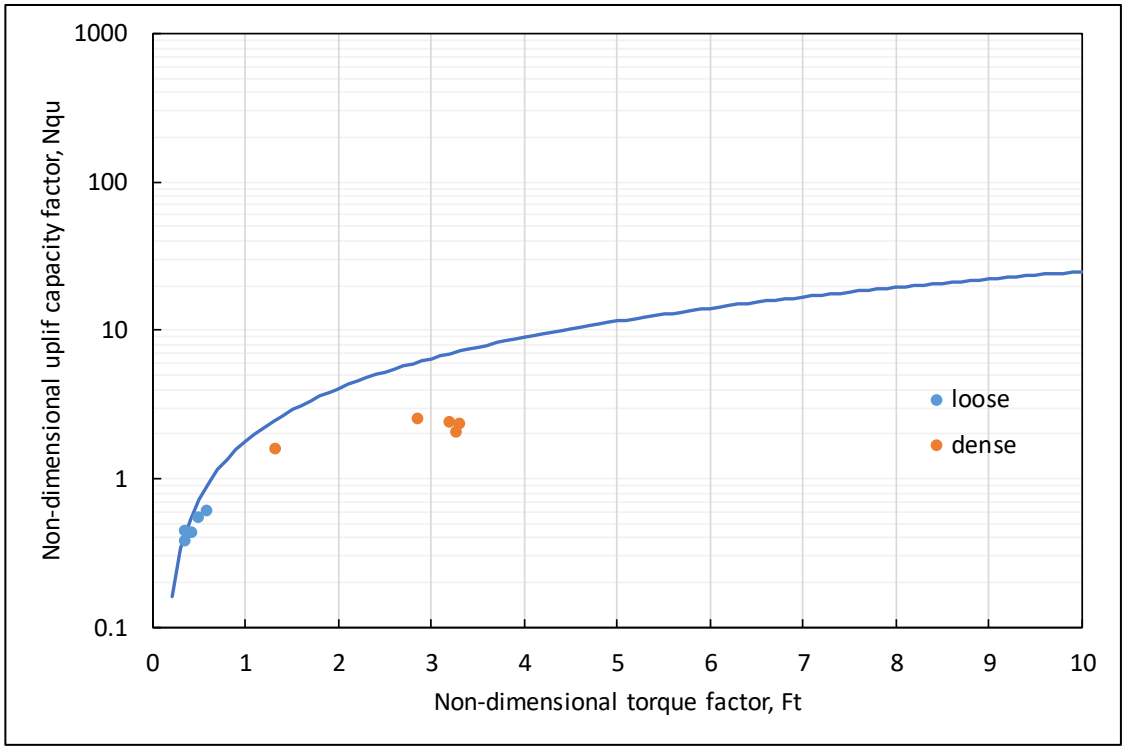

Figure 28: Plot of the equation provided by Ghaly and Hanna (1991)

It was not possible to reproduce the plot of Ghaly and Hanna (1991). A plot of their equation in Figure 28 is slightly different than in their paper shown previously in Figure 6. The error is higher as the torque factor increases. It can be observed, that the loose dimensionless factors match the equation well, while the dense test results plot lower than the equation. It is important to note, however, that the uplift capacity factor is on a log scale so differences appear smaller than they actually are. For example, the dense tests were off by a factor of about 3.

Overall, the model overpredicts the torque and the uplift capacity in all cases, especially for loose sand conditions. However, it predicts the required torque value for the plain steel anchor in dense sand almost exactly, but not the uplift capacity. Hence, in this case

the error in torque factor would be due to the poor prediction of the pullout capacity. One approach to improving the predictions, therefore, is to combine their torque model with an improved model for pullout capacity.

The installation model was not accurate for the jetted installation method, since the predicted value is higher by a factor of 2.5. It is possible that the jetting method may be decreasing the lateral stresses in the soil. To investigate this effect, the modified coefficient of passive earth pressure (K_p') in the equation for the resisting moment at the shaft (T_1) was replaced by a value for at rest conditions (equation 12):

(12) $$K_0 = 1 - \sin(\Phi)$$

where Φ is the peak friction angle of the dense sand 42.7°.

K_0 was calculated to be 0.32 which is 1/5 of the K_p' value. This led to an 80% decrease for T_1 but only a decrease of 8% in the overall required installation torque, and a minimal decrease in the calculated torque factor. This is because the shaft resistance only represents 10% of the overall resistance. For loose sand, the given ranges are comparable. Regarding this fact, the model may not be able to capture the jetted installation method.

4.4 Tsuha & Aoki: Power Screw Model

The model developed by Tsuha & Aoki (2010) assumes that the required installation torque (T) is the sum of the resisting moments of the shaft (T_S) and the helices (T_h). The ultimate uplift capacity (Q_u) can be calculated in a similar way by addition of the shaft resistance (Q_s) and the uplift helix bearing capacity (Q_h). In their study, the shaft resistance was not verified because of the risk of scale effect, which occur for shaft diameters smaller than $200D_{50}$ (where D_{50} is the average grain size). In the present study, the ratio of external diameter (d=45.7 mm) to average grain size is 152, what indicates that scale effects may be present. Also, Tsuha & Aoki installed piles for each series without helical blades, just as a shaft. They found out, that the uplift capacity and the installation torque associated with the resistance on the pile shaft, were not significant compared with the helix contribution. Based on this statement they only used Q_h and T_h for their modeling and further calculations for the torque factor, where T_h represents the measured torque at the end of the installation process. They validated the derived equations using centrifuge tests, which allows the effective stresses in the soil to be scaled. However, the resisting moment and the pullout resistance of the plain shaft were subtracted from all test results to obtain appropriate data for the helix contribution. Hence, the model only provides a torque factor for the helix and not for the whole helical pile.

As a first step an analysis was performed for the test data presented in Tsuha and Aoki (2010) and the results could be replicated.

4.4.1 Calculations

After dividing Q_h by T_h, the equation for the torque factor is as follows:

(13) $K_{Th} = \left[\frac{2}{d_c \tan(\theta+\delta_r)}\right]$,

[13a] $\theta = \tan^{-1}\left(\frac{p}{\pi d_c}\right)$,

[13b] $d_c = \frac{2}{3} * \left(\frac{D^3-d^3}{D^2-d^2}\right)$,

where d_c=helix surface area, θ= helix angle, and δ_r=residual interface friction angle, p=pitch, D=outer blade diameter, and d=outer shaft diameter.

Clearly, the equation indicates that the torque factor only depends on the helix geometry and the interface friction angle. Note that the equation does not consider the torque and capacity associated with the friction on the shaft. Therefore, to be consistent with the model predictions it is necessary to subtract out the shaft resistances from the measured test data. Since there are no tests that quantify the shaft contribution, simple static capacity models are used to calculate the part of the resisting torque and the uplift resistance of the shaft. For the uplift shaft resistance, the "beta" method was used (Hannigan, 2006).

(14) $Q_S = \frac{1}{3} A_S * K_S \tan\delta_r \, \sigma_{v,a}$

where A_s is the area of the shaft surface, K_S is the coefficient of earth pressure, and $\sigma_{v,a}$ is the average effective overburden earth pressure at the middle of the shaft.

Equation 15 was derived to estimate the torque resistance on the shaft:

(15) $T_S = \gamma D^2 K_S \tan\delta_r \, r_0^2$

where γ is the unit weight of the sand sample, D is the installation depth between soil surface and the top of the helical blade, and r_0 is the outer radius of the shaft.

Since the lateral earth pressure plays an important role regarding the calculation of the shaft resistance, high and low values were taken to calculate the resistances. The high and low values are reflected indirectly later, by comparing the results of the model. The values were chosen based on approximate ratios of coefficients of lateral earth pressure after construction (K) to that before construction (K_0) of driven piles (Coduto 2001). For the normal installation method, a driven large displacement pile was considered and a low-displacement pile was assumed for the jetted installation method. A nominal value of 0.4 was assumed for K_0 and used to calculate K. The high and low values are summarized in Table 16.

Table 16: Summary of chosen K values for normal and jetted installation method

	Low K	*High K*
Normal installation	0.4	0.8
Jetted	0.3	0.5

The K values were chosen from Table 16 and used in equations 14 and 15 to get upper and lower bound estimates for the shaft contribution. For the residual interface friction angle, the results of the steel interface shear tests were taken. Table 17 summarizes the results for the shaft resistances.

Table 17: Shaft contribution for pile pullout and moment resistance calculated for low and (high) K values

	Loose		*Dense*	
	Closed	*Jetted*	*Closed*	*Jetted*
Shaft pullout resistance, Qs [N]	81.5 (162.9)	61.1 (101.8)	89.6 (179.2)	67.2 (112.0)
Shaft resisting torque, Ts [Nm]	1.8 (3.6)	1.3 (2.2)	2.0 (3.91)	1.5 (2.4)

It can be observed, that the coefficient of the earth pressure causes a significant difference and is very sensitive in these equations. It is noted that the chosen values are just an assumption based on a range, since the exact values were not measured. As Tsuha and Aoki mentioned, the shaft resistances are small compared to the helical part. For this data set they are roughly in the range of 4-12 % for loose and just 1-2 % for dense sand. Table 18 shows the corrected measured values of the own pile tests from chapter 4.1.

Table 18: Summary of pile load test data adjusted to remove the effects of shaft resistance.

Pile	*Average Torque, T_h [Nm]*	*Pullout Load, Q_h [N]*	*Torque Factor, $K_{T,h}$ [m^{-1}]*
Loose (D_r= 27 %)			
LPC1 (steel)	26 (24)	1718 (1637)	66 (68)
LRC1 (sandpaper)	31 (29)	1919 (1837)	61 (62)
LSC1 (Teflon)	21 (20)	1368 (1287)	78 (82)
LSC2 (Teflon)	18 (16)	1368 (1287)	67 (82)
LJO1 (“jetted”)	18 (17)	1188 (1188)	67 (68)
Dense (D_r= 65 %)			
DPC1 (steel)	202 (200)	8610 (8520)	43 (43)
DPC2 (steel)	206 (204)	7410 (7320)	36 (36)
DRC1(sandpaper)	208 (206)	8460 (8370)	41 (41)
DSC1 (Teflon)	180 (178)	9010 (8920)	50 (50)
DJO1 (“jetted”)	82 (81)	5718 (5718)	69 (70)

It can be observed, that the correction gives variations of -2.2 to +3 % for the torque factor for loose and for dense sand it alternates just between -1.1 and +0.7 %. This emphasizes the fact, that the shaft resistances are not significant regarding the whole pile resistance and do not lead to major variations.

After correcting the test data, equation 13 was used to predict the torque factor. The pile properties provided in chapter 4.1 and the installation torques in table 18 were used.

4.4.2 Results and Discussion

Figure 29 shows a comparison between the corrected measured and the predicted torque factor K_{th}, for both high and low K values.

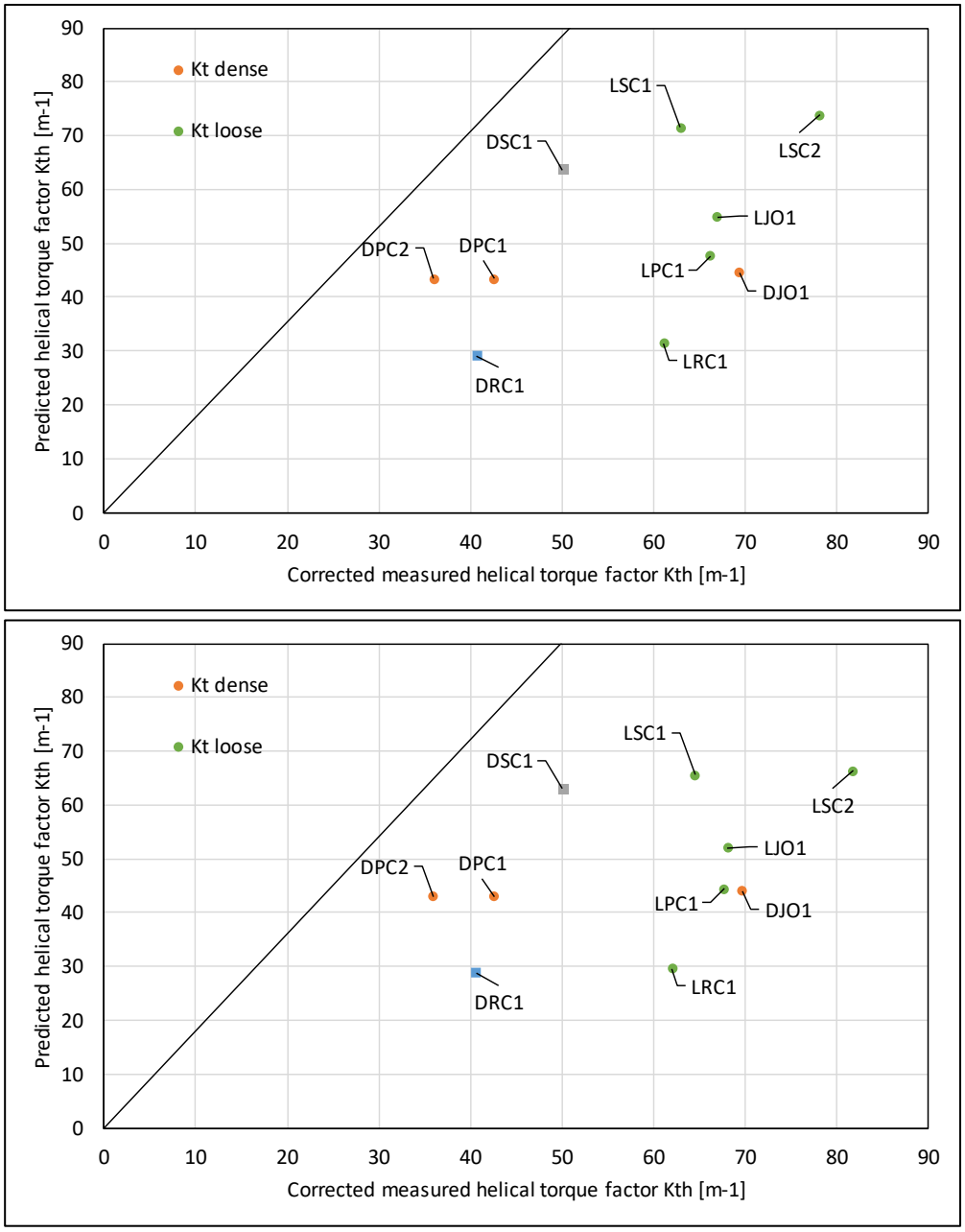

Figure 29: Comparison between corrected measured and predicted helical torque factor K_T for low (top) and high (bottom) K values

It can be observed, that the model tends to overpredict the torque factor in general. The dense steel test one is predicted almost exactly, while the second one is overpredicted by factor 1.19, and jetted is underpredicted by 0.63. The predictions for Teflon and

sandpaper in the dense sand cannot be considered accurately because the attached sheets ripped off during the test runs. The change in K value causes no significant changes to the torque factor for dense sand. The loose tests vary by factors between 0.51 and 1.15, whereby all of them overpredict the torque factor except for the first Teflon test. The change of K leads to visible changes in the torque factor for loose sand. The torque factors for low K values approach the 1:1 ratio a little better than for the high K values. For high K values, all data points shift to the right and away from the diagonal line, while the data points for the low K are closer.

A comparison of both steel and Teflon test results (for low K values, for example) shows, that the variances can also be due to variability in the tests, since the first test series data gives an almost 1:1 prediction, while the second is off by a variance in the factor of 0.2. The variability in the predicted values for the jetted (dense) shows, that the installation process may provide different conditions that cannot be captured by the model. For the loose sand tests, the model underpredicts in most cases. Also, the change in K causes a visible change for the predicted torque factor, while it almost changes nothing for the dense tests. For example, an increase of 100% of K for the loose Teflon tests causes a 13% difference, while it just causes a 1% increase for the dense steel tests. This indicates that the shafts contribution for the resistance is relatively higher for the loose than it is for the dense sand, but it is still relatively small.

The results were analyzed further to see if the penetration rate might explain the differences in the predicted and measured torque factors (Figure 30).

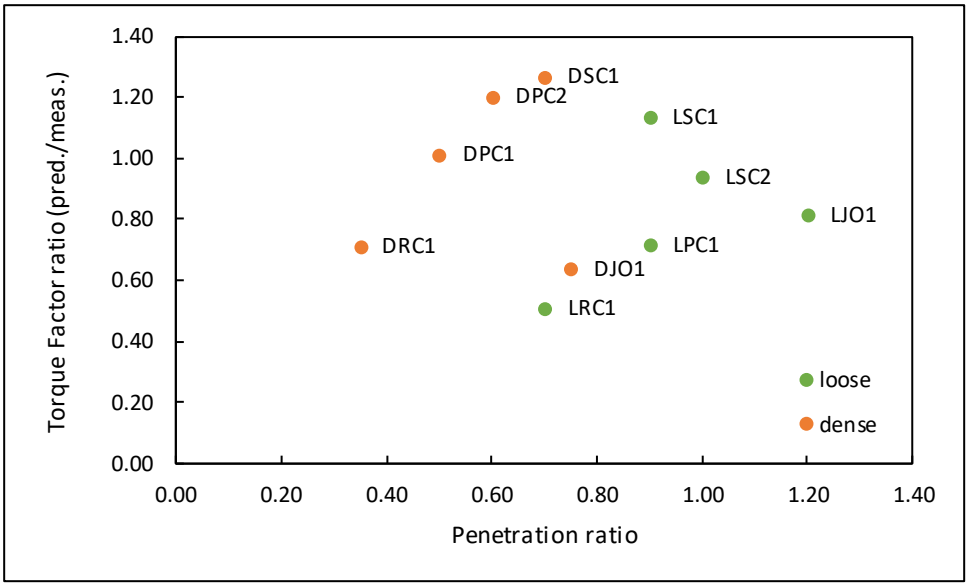

Figure 30: Penetration ratio vs. torque factor ratio

The penetration ratio indicates either if the pile under or over penetrates during the installation. A penetration ratio of 100% means that in one revolution the anchor has penetrated downward a distance equal to the helix pitch. A perfect penetration ratio could lead to better predictions of the model since it is based on power screws but comparing all results and the ratios does not give any relationship or trends.

However, it seems like the model could give relatively good predictions and can be used at least to get a rough range for the torque factor. This may be because the models' torque factor strongly depends of the interface friction angle, which changed within the helical pile test series. Hence, this model may be useful for predictions in case of

improving helical pile efficiency by modifying the roughness of the helical anchor plate surface.

4.5 Summary

Figure 31 shows a comparison between the ratio of predicted over measured torque factor of all applied models.

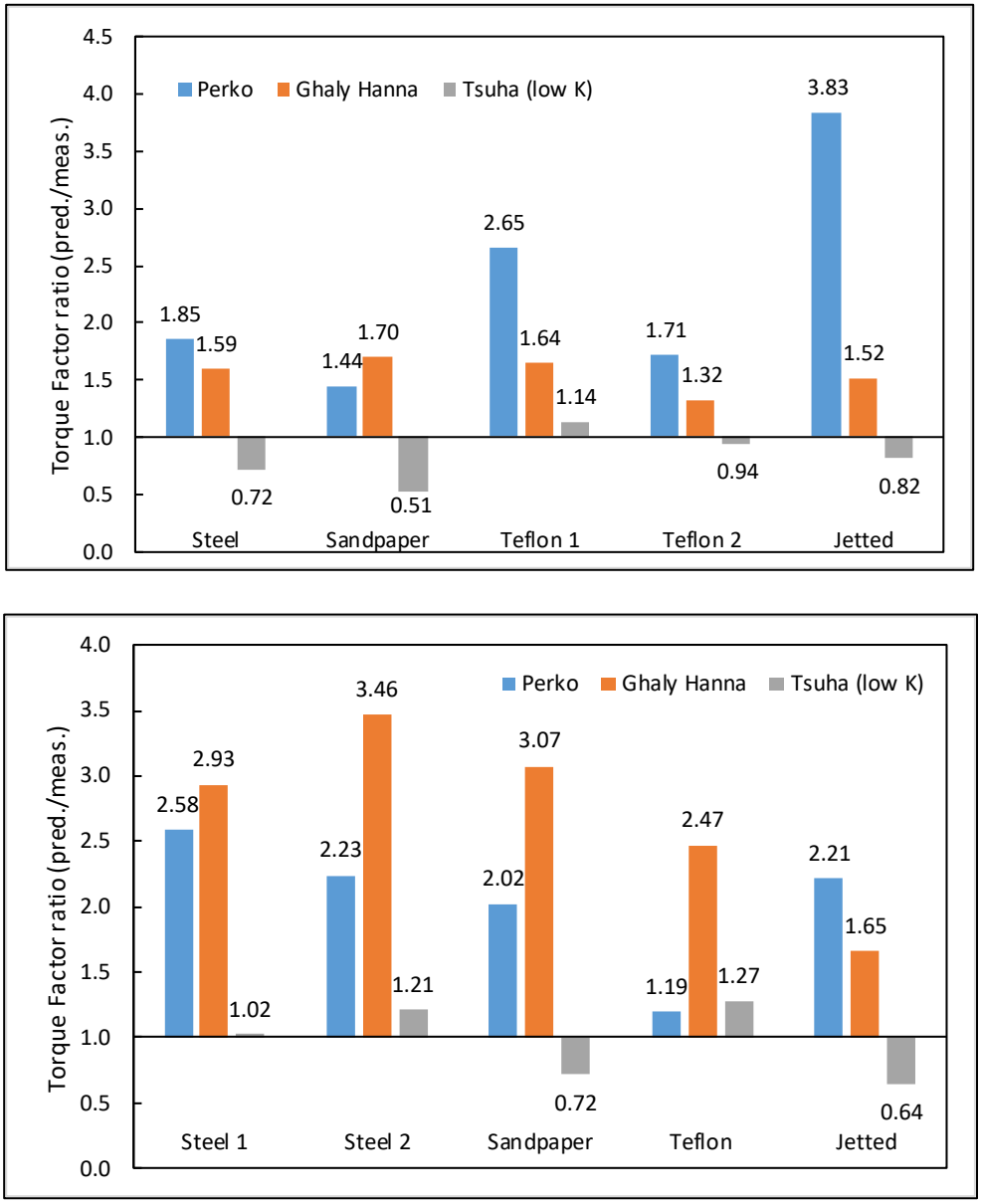

Figure 31: Comparison between predicted and measured torque factors of all models for loose (top) and dense (bottom) sand

For the calculated torque factor from Ghaly and Hanna equation 9 was used for the comparison. It is noted, that the Tsuha and Aoki ratios only represent the helical blade torque factor. The ratios for low K were chosen, since they give better results. In Figure 33 a bias ratio of 1 would indicate a perfect prediction. Overall, the models by Ghaly & Hanna and Perko tend to overpredict the actual torque factor, while Tsuha's model provides very good predictions on average. The ratios for Perko spread widely, especially for loose sand from 1.44 to 3.83, while they are around a level of 2 for dense sand, except for Teflon. Ghaly's predictions for loose sand vary between 1.32 and 1.70, and for dense between 1.65 and 3.46. The best predictions are made by Tsuha's model in loose sand, which vary within a range of 0.51 and 1.21.

Perko's model uses the work done during installation and pullout. Many input parameters are necessary, but some of the properties appear to be empirical. The model is very sensitive for small changes in the input data, for example, the vertical displacement for the peak pullout capacity. This value had a wider range for the loose tests, and hence the variation in the predicted torque factors is more significant.

Ghaly and Hanna only provide a model in form of a non-dimensional equation which correlates measured installation torques to uplift capacities, since their main research focuses the prediction of required installation torques. The correlation seems to be more reasonable for lower installation torques in loose sand, while the variance increases for higher torque values in dense sand, what is also reflected by the jetted installation process having a lower required installation torque, as well as the loose Teflon 2 test

having the lowest torque. This leads to the assumption that an adjustment factor may be necessary.

The best prediction is provided by Tsuha and Aoki's model. It focuses the forces arising at the helical blade and considers the interface friction angle as a main input parameter. Hence, it provides a torque factor that only depends on helical blade interface properties and dimensions. It was most accurate for the plain steel anchors in dense and for the Teflon coated anchors in loose sand. Some uncertainties result from the earth pressure assumptions that had to be made to remove the shaft friction from the load test data. The comparison of upper and lower bound values for K shows that the loose sand is significantly more sensitive to changes in K than the dense sand. The lateral stress is discussed in the literature, and especially for the jetted installation process, the coefficient could change a lot. Overall, Tsuha's model tends to give the most reasonable results, but can still give variations of up to 52 %.

CHAPTER 5: SUMMARY & CONCLUSIONS

5.1 Summary

The objective of this thesis was to evaluate three different models from the literature in their prediction of a torque factor for a deeply embedded helical pile. This was accomplished by comparing the model predictions to the results of 1/5-scale physical model tests performed on a helical pile in sand. In an attempt to improve their geotechnical efficiency, the helical piles were modified by changing the roughness of the helical plate as well performing a jetting operation to avoid the formation of a soil plug within the shaft. First, a suite of interface shear tests was conducted, to obtain the residual interface friction angles between the test sand and the tested materials, used in the helical pile tests. Three different models were used to predict the installation forces and/or torque factor in the physical model tests and they were compared to the measured results.

5.2 Conclusions

The following conclusions can be made:

- Three analytical models were identified in the literature that could be used to predict the torque factor of a helical pile. One that is based on energy concepts (Perko 2001), one that is based on forces on a free body diagram combined with earth pressure theory (Ghaly and Hanna 1991), and a third that uses mechanics principles for a power screw (Tsuha and Aoki 2010).
- A modified direct shear test was successfully used to measure the residual interface friction angle of sand. Residual interface friction angles between Westerly sand and steel, sandpaper, and Teflon were calculated to be 23.2°, 33.3°, and 15.5°, respectively.
- The results indicate that the energy-based model by Perko (2001) overpredicts the torque factor in most cases. The model is difficult to apply with any confidence because two of the input parameters appear to be empirical and not a fundamental soil or mechanical property.
- Ghaly and Hanna's model overpredict the measured test results, especially in dense conditions by a factor of 1.65 to 3.46, in contrast to loose conditions by a factor of 1.32 to 1.70. The equations provided to calculate the required installation torque largely overpredicted in loose sand but give very good results for the steel piles installed in dense sand. However, the jetted installation method causes changes to the soil that cannot be captured by the model.
- The model by Tsuha and Aoki (2010) gave the best predictions of torque factor. The ratio of predicted over measured ranges from 0.62 to 1.19 and the closest

predictions are made for the dense steel (1.0 and 1.19) and the loose Teflon (0.96 and 0.75) tests. Overall, the model, considering mainly the residual interface friction angle and helical anchor size, appeared to capture the observed behavior of the helical pile.

5.3 Further Studies

A focus should be put on the conduction of the interface shear tests, since they show some variances in the reproducibility, especially for steel. The issue of the sand loss during the tests could be fixed by a larger shear box where the sand loss does not lead to significant changes in volume change because of the greater volume.

Furthermore, it seems like models using theoretically based models (e.g., power screw model) give better predictions than those relying only on empirical bases like the Ghaly and Hanna equation. Hence, a focus should be put on theoretical models.

APPENDICES

A. Screenshots of made settings for the shear test device software

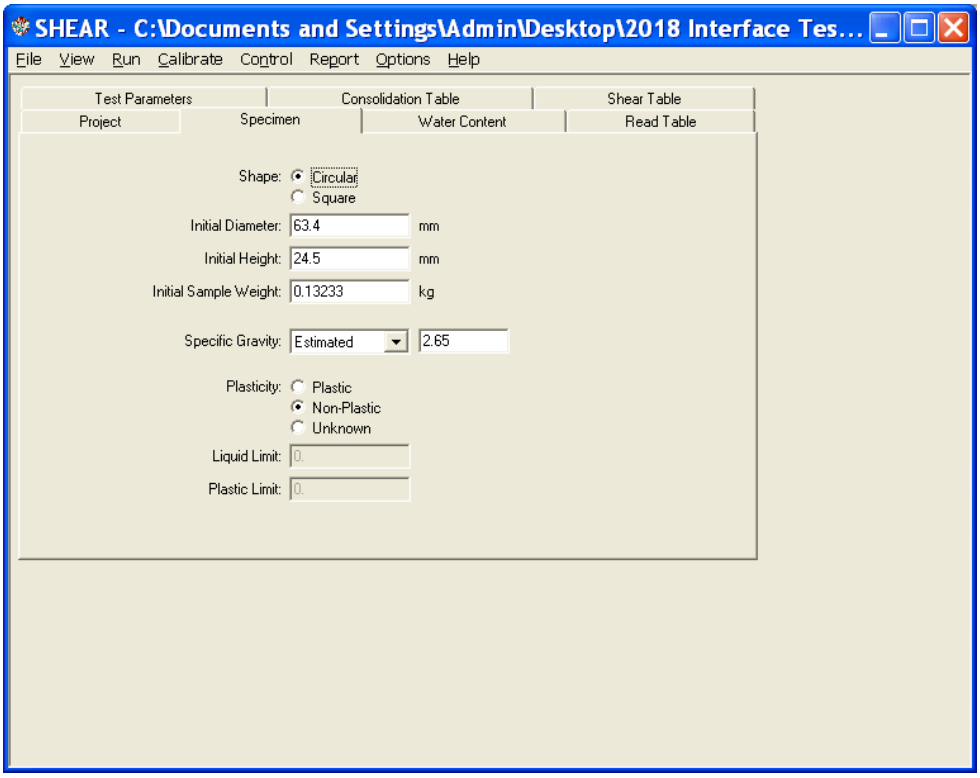

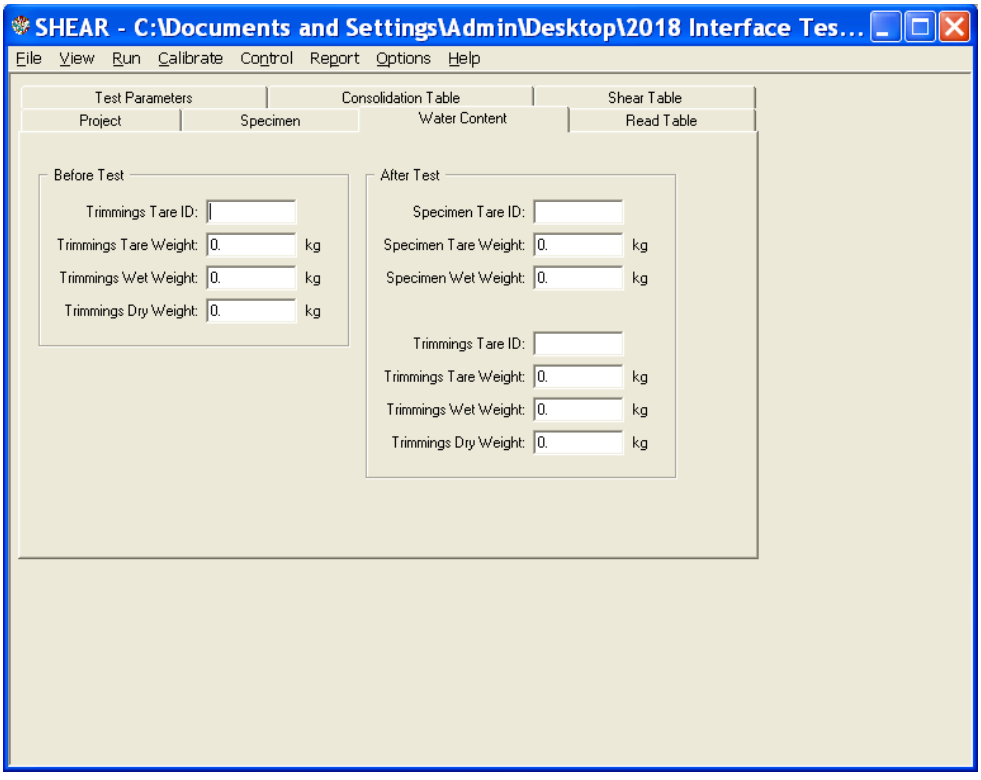

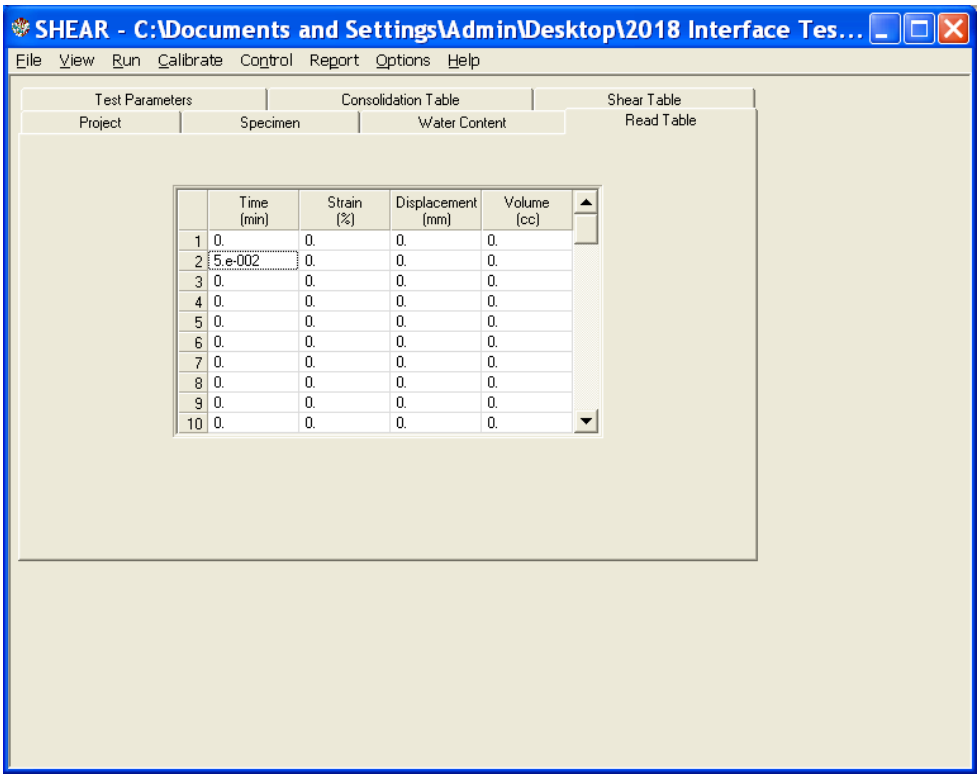
SHEAR - C:\Documents and Settings\Admin\Desktop\2018 Interface Tes...
File View Run Calibrate Control Report Options Help
Test Parameters
Consolidation Table
Shear Table
Project
Specimen
Water Content
Read Table
Time (min)
Strain (%)
Displacement (mm)
Volume (cc)
1 0. 0. 0. 0.
2 5.e-002 0. 0. 0.
3 0. 0. 0. 0.
4 0. 0. 0. 0.
5 0. 0. 0. 0.
6 0. 0. 0. 0.
7 0. 0. 0. 0.
8 0. 0. 0. 0.
9 0. 0. 0. 0.
10 0. 0. 0. 0.

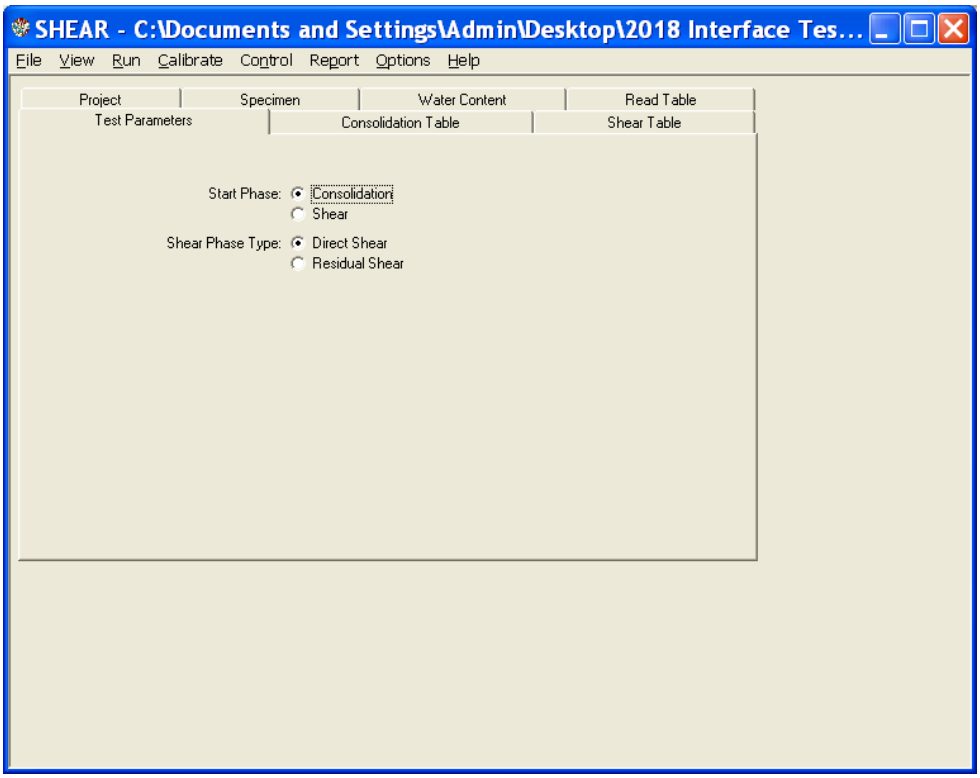
SHEAR - C:\Documents and Settings\Admin\Desktop\2018 Interface Tes...
File View Run Calibrate Control Report Options Help
Project
Specimen
Water Content
Read Table
Test Parameters
Consolidation Table
Shear Table
Start Phase:
Consolidation
Shear
Shear Phase Type:
Direct Shear
Residual Shear

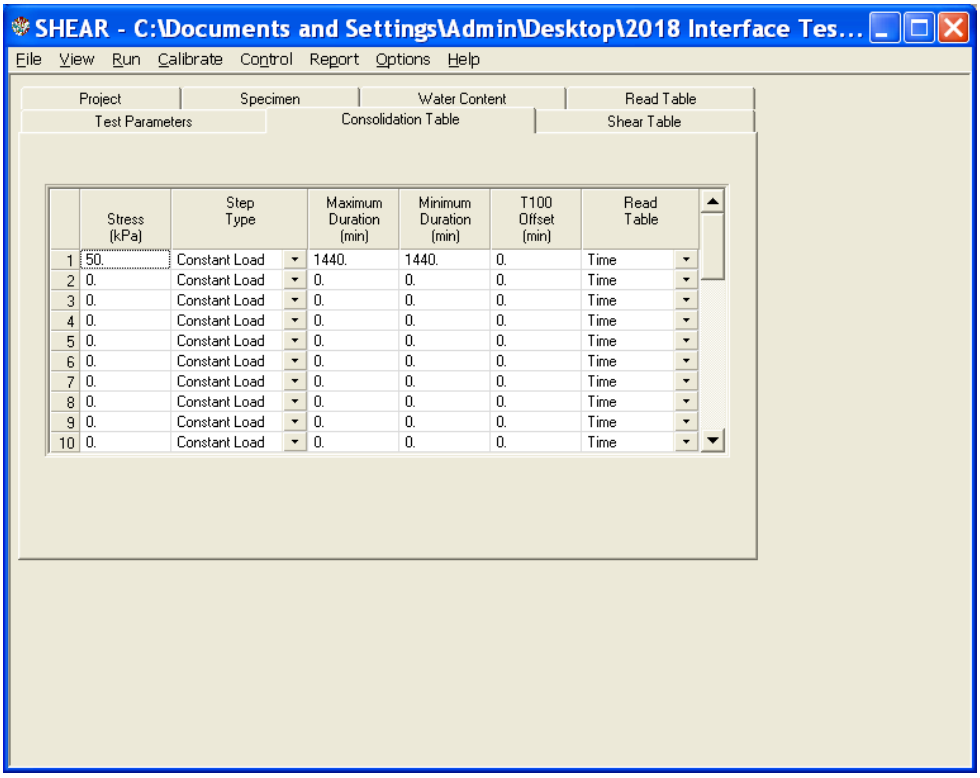
SHEAR - C:\Documents and Settings\Admin\Desktop\2018 Interface Tes...
File View Run Calibrate Control Report Options Help
Project Specimen Water Content Read Table
Test Parameters Consolidation Table Shear Table
Stress (kPa) | Step Type | Maximum Duration (min) | Minimum Duration (min) | T100 Offset (min) | Read Table
1 50. Constant Load 1440. 1440. 0. Time
2 0. Constant Load 0. 0. 0. Time
3 0. Constant Load 0. 0. 0. Time
4 0. Constant Load 0. 0. 0. Time
5 0. Constant Load 0. 0. 0. Time
6 0. Constant Load 0. 0. 0. Time
7 0. Constant Load 0. 0. 0. Time
8 0. Constant Load 0. 0. 0. Time
9 0. Constant Load 0. 0. 0. Time
10 0. Constant Load 0. 0. 0. Time

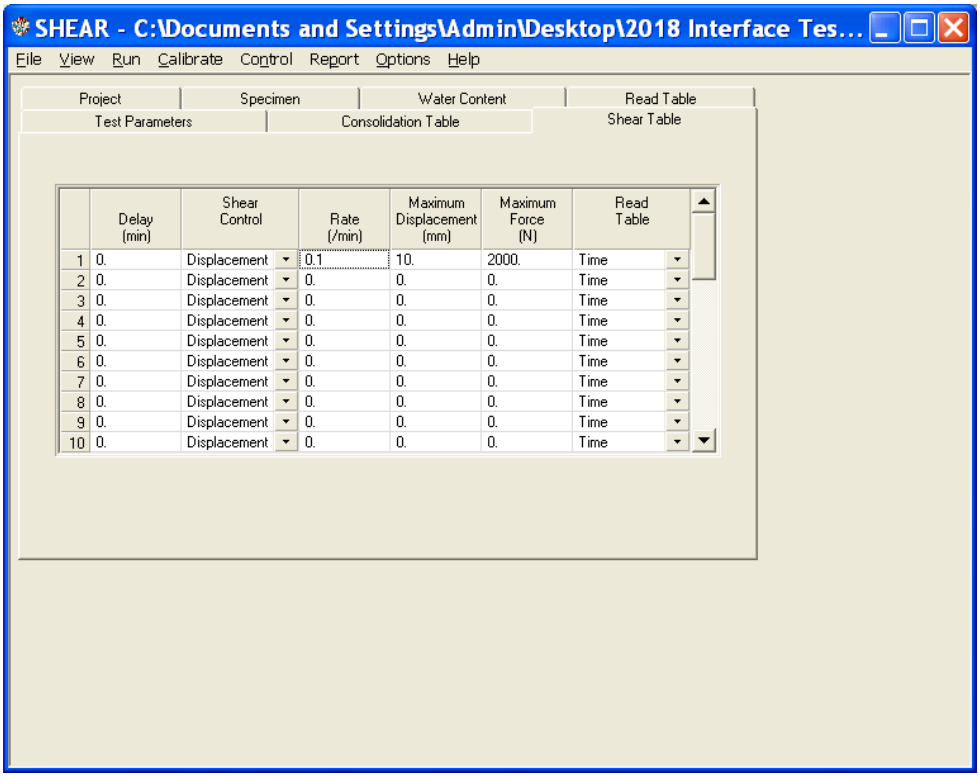
SHEAR - C:\Documents and Settings\Admin\Desktop\2018 Interface Tes...
File View Run Calibrate Control Report Options Help
Project Specimen Water Content Read Table
Test Parameters Consolidation Table Shear Table
Delay (min) | Shear Control | Rate (/min) | Maximum Displacement (mm) | Maximum Force (N) | Read Table
1 0. Displacement 0.1 10. 2000. Time
2 0. Displacement 0. 0. 0. Time
3 0. Displacement 0. 0. 0. Time
4 0. Displacement 0. 0. 0. Time
5 0. Displacement 0. 0. 0. Time
6 0. Displacement 0. 0. 0. Time
7 0. Displacement 0. 0. 0. Time
8 0. Displacement 0. 0. 0. Time
9 0. Displacement 0. 0. 0. Time
10 0. Displacement 0. 0. 0. Time

B. Calculation of Peak Friction Angles (Bradshaw & Giampa (2018)

The peak friction angles were calculate using equation 16:

(16) $\Phi'_p = A_f I_R + \Phi'_c$

[16a] $I_R = I_D\left[\left(Q_1 + \Delta Q \ln\left(p'_f\right)\right) - \ln\left(p'_f\right)\right] - R$

where Φ'_p is the peak friction angle, Φ'_c is the critical state friction angle, I_D is the relative sand density, p'_f is the mean effective confining pressure at failure (=installation depth * sand density), I_R is the relative dilatancy index, and A_f, Q_1, ΔQ, R are soil specific constants. The calculation is summarized in Table 19 below.

Table 19: Calculation of the peak friction angle for Westerly sand

	loose	*dense*
γ [kN/m3]	15	16.5
I_D	0.2743	0.6560
Q_1	3.89	3.89
ΔQ	0.66	0.66
p'_f [kPa]	17.25	18.98
R	-0.28	-0.28
A_f	4.8	4.8
Φ'_c [°]	32.3	32.3
Ir	1.08	2.18
Φ'_p [°]	**37.5**	**42.7**

BIBLIOGRAPHY

Clemence, S.P., Crouch, L.K., and Stephenson, R.W. (1994). "Prediction of Uplift Capacity for Helical Anchors in Sand." Second Geotechnical Engineering Conference, Cairo, Egypt, Vol. I, pp. 332-343.

Coduto, D. P. (2001). Foundation design: principles and practices. Prentice Hall, Upper Saddle River, N.J.

Ghaly, A., and Hanna, A. (1991). “Experimental and theoretical studies on installation torque of screw anchors.” Canadian Geotechnical Journal, 28(3), 353–364.

Giampa, J. R., and Bradshaw, A. S. (2018). “A Simple Method for Assessing the Peak Friction Angle of Sand at Very Low Confining Pressures.” Geotechnical Testing Journal, 41(4).

Hannigan, P. J. (2006). “Design and construction of driven pile foundations: Reference manual.”, p. 9-81.

Hoyt, R.M., and Clemence, S.P. (1989). “Uplift Capacity of Helical Anchors in Soil.” 12th International Conference on Soil Mechanics and Foundation Engineering, Rio de Janeiro, Brazil.

Perko, H. A. (2000). “Energy Method for Predicting Installation Torque of Helical Foundations and Anchors.” New Technological and Design Developments in Deep Foundations.

Olson, R. E., and Lai, J. (2004). “Direct Shear Testing”. https://www.cyut.edu.tw/~jrlai/CE7334/Unit3.pdf (August 30, 2018).

Tsuha, C. D. H. C., and Aoki, N. (2010). “Relationship between installation torque and uplift capacity of deep helical piles in sand.” Canadian Geotechnical Journal, 47(6), 635–647.

Uesugi, M., and Kishida, H. (1986). “Frictional resistance at yield between dry sand and mild steel.” Soils And Foundations, 26(4), 139–149.

Suits, L. D., Sheahan, T., Porcino, D., Fioravante, V., Ghionna, V., and Pedroni, S. (2003). “Interface Behavior of Sands from Constant Normal Stiffness Direct Shear Tests.” Geotechnical Testing Journal, 26(3), 19513.

Zuelke, R. (2018). “Improving Helical Anchor Efficiency: An Experimental Study.” University of Rhode Island.